Electroweak corrections to $W + \mathrm{jet}$ hadroproduction including leptonic W-boson decays

Ansgar Denner,[a] **Stefan Dittmaier,**[b,c] **Tobias Kasprzik**[c] **and Alexander Mück**[a]

[a] *Paul Scherrer Institut, Würenlingen und Villigen,*
Ch-5232 Villigen PSI, Switzerland

[b] *Albert-Ludwigs-Universität Freiburg, Physikalisches Institut,*
D-79104 Freiburg, Germany

[c] *Max-Planck-Institut für Physik (Werner-Heisenberg-Institut),*
D-80805 München, Germany

E-mail: ansgar.denner@psi.ch,
stefan.dittmaier@physik.uni-freiburg.de, tobiask@mppmu.mpg.de,
mueck@physik.rwth-aachen.de

Abstract: We present the first calculation of the next-to-leading-order electroweak corrections to W-boson + jet hadroproduction including leptonic W-boson decays. The W-boson resonance is treated consistently using the complex-mass scheme, and all off-shell effects are taken into account. The corresponding next-to-leading-order QCD corrections have also been recalculated. All the results are implemented in a flexible Monte Carlo code. Numerical results for cross sections and distributions of this Standard Model benchmark process are presented for the Tevatron and the LHC.

Contents

1 Introduction

The production of electroweak (EW) W and Z bosons with subsequent leptonic decays is one of the most prominent Standard Model (SM) processes at present and future hadron colliders like the Tevatron and the LHC. The signatures are clean owing to the final-state leptons, and the cross sections are large. The (expected) experimental accuracy is so excellent that the charged-current Drell-Yan process allows to improve the precision measurement of the W-boson mass. Moreover, it can deliver important constraints in the fit of the parton distribution functions (PDFs) and may serve as a luminosity monitor at the LHC. The off-shell tails of appropriate distributions give access to a W-width measurement and, at high energies, offer the possibility to search for new charged W′ gauge bosons. (See e.g. ref. [1, 2] and references therein.)

At hadron colliders, the EW gauge bosons are (almost) always produced together with additional QCD radiation. The production cross section of W bosons in association with a hard, visible jet,

$$\mathrm{pp/p\bar{p}} \rightarrow \mathrm{W} + \mathrm{jet} \rightarrow l\nu_l + \mathrm{jet} + X, \tag{1.1}$$

is still large. Moreover, the intermediate W boson recoils against the jet leading to a new kinematical situation with strongly boosted W bosons. For large transverse momentum (p_T) of the jet the corresponding events contain charged leptons and/or neutrinos with large

– 1 –

p_{T}. In fact, in the SM, W + jet(s) production is the largest source for events with large missing transverse momentum where also a charged lepton is present for triggering. Hence, W + jet(s) production is not only a SM candle process. It is also an important background for a large class of new physics searches based on missing transverse momentum. Moreover, the process offers the possibility for precision tests concerning jet dynamics in QCD.

To match the prospects and importance of this process class, an excellent theoretical prediction is mandatory. The differential cross section for W-boson production is known at NNLO accuracy with respect to QCD corrections [3] and even up to N^3LO in the soft-plus-virtual approximation [4]. The next-to-leading-order (NLO) QCD corrections have been matched with parton showers [5] and combined with a summation of soft-gluon radiation (see e.g. ref. [6]), which is particularly important to reliably predict the transverse-momentum distribution of the W bosons for small p_{T}. A theoretical study of the QCD uncertainties in the determination of the W cross section at hadron colliders has been presented in ref. [7]. Concerning EW corrections, the full NLO [8–11] and leading higher-order effects, in particular due to multi-photon final-state radiation [11–14], have been calculated. The contributions of photon-induced processes have been discussed in refs. [14–16]. First steps towards combining QCD and EW higher-order effects have been taken in ref. [17]. The NLO QCD and EW corrections have been also calculated within the MSSM [14].

The cross section for W + 1 jet [18, 19] and W + 2 jets [19] production is known at NLO QCD. The calculation of the NLO QCD corrections in the leading-colour approximation for the W + 3 jets cross section has recently been completed [20].

So far, the EW corrections in the SM have been assessed for W + 1 jet production in the approximation where the W boson is treated as a stable external particle [21–23] (see ref. [24] for an MSSM analysis). For W bosons at large transverse momentum, i.e. at large centre-of-mass energy, this is a good approximation since the EW corrections are dominated by large universal Sudakov logarithms [25]. However, an on-shell calculation cannot assess any off-shell effects due to the finite width of the W boson and is blind to the details of the experimental event selection based on the charged-lepton momentum and the missing transverse momentum of the neutrino.

In this work, we present a calculation of the NLO EW corrections for the physical final state in W-boson hadroproduction, i.e. $\mathrm{pp}/\mathrm{p\bar{p}} \to l\nu_l + \mathrm{jet} + X$. The W resonance is described in the complex-mass scheme [26, 27]. All off-shell effects due to the finite width of the W boson are included. Our results have been implemented in a fully flexible Monte Carlo code which is able to calculate binned distributions for all physically relevant W + 1 jet observables. In real emission events with photons inside a jet, we distinguish W + jet and W + photon production by a cut on the photon energy fraction inside the jet employing a measured quark-to-photon fragmentation function [28].

Our calculation is completely generic in the sense that it can predict observables which are dominated by W bosons close to their mass shell as well as observables for which the exchanged W boson is far off-shell. The calculation of the EW corrections for W production in association with a hard jet is also a step towards a better understanding of the interplay between QCD and EW corrections for W production in general. This understanding — including a full treatment of off-shell W bosons — is mandatory to match the envisaged experimental accuracy for the W-mass measurement at the Tevatron and the LHC.
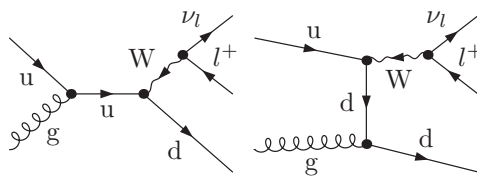
Figure 1. Feynman diagrams for the LO process (2.2).

To reach the accuracy of $\mathcal{O}(\alpha_s\alpha^3)$ throughout the calculation we have also included the photon-induced partonic processes and the respective NLO QCD corrections. Also non-trivial interference terms between EW and QCD diagrams within the real corrections have been included at this order. Moreover, we have recalculated the NLO QCD corrections at $\mathcal{O}(\alpha_s^2\alpha^2)$ in a fully flexible way, supporting a phase-space dependent choice for the factorization and renormalization scales.

This paper is organized as follows. In section 2, we describe our calculation in detail and discuss all the theoretical concepts and tools which have been used. In section 3, we specify the numerical input as well as the details of our event selection. Numerical results are given for W^+ production both at the LHC and at the Tevatron. We present inclusive cross sections for specified sets of cuts as well as distributions for the relevant observables. We conclude in section 4.

2 Details of the calculation

2.1 General setup

The hadroproduction of a W boson in association with one hard jet is governed at leading order (LO) by quark-antiquark fusion, where the initial-state quarks radiate a gluon, and the corresponding crossed channels with a gluon in the initial state. Specifically, for W^+ production the relevant partonic processes are

$$u_i\,\bar{d}_j \rightarrow W^+g \rightarrow l^+\nu_l\,g\,, \tag{2.1}$$

$$u_i\,g\, \rightarrow W^+d_j \rightarrow l^+\nu_l\,d_j\,, \tag{2.2}$$

$$\bar{d}_j\,g\, \rightarrow W^+\bar{u}_i \rightarrow l^+\nu_l\,\bar{u}_i\,, \tag{2.3}$$

where u_i and d_j denote an up-type quark of generation i and a down-type quark of generation j, respectively. We perform the calculation for the physical final state, i.e. a charged lepton l, the corresponding neutrino ν_l, and a parton which will be seen in the detector as a jet. The corresponding tree-level Feynman diagrams for process (2.2) are shown in figure 1. The intermediate W-boson resonance is described by a complex W-boson mass μ_W via the replacement

$$M_W^2 \rightarrow \mu_W^2 = M_W^2 - iM_W\Gamma_W \tag{2.4}$$

in the W propagator as dictated by the complex-mass scheme (see below). Hence, all our results correspond to a fixed-width description of the Breit-Wigner resonance.
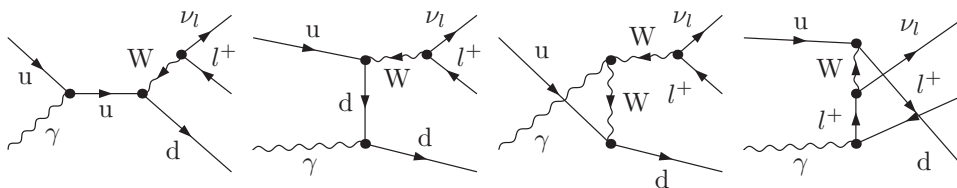
Figure 2. Feynman diagrams for the photon-induced process (2.5).

The leptons are treated as massless unless their small masses are used to regularize a collinear divergence.

The dependence on quark mixing, as parametrized in the CKM matrix, factorizes from the tree-level matrix elements. Apart from a global CKM-dependent factor, the tree-level amplitudes do not depend on the specific flavours. Hence, for hadronic observables, the summation over the quark flavours $i = 1, 2$ and $j = 1, 2, 3$ requires only the evaluation of a single generic amplitude per process type shown in (2.1)–(2.3) when folding the squared tree-level amplitudes with the corresponding PDFs. Only squares of the absolute value of CKM elements enter the final results. We do not include top quarks in the final state since their decays lead to significantly different signatures. The five other quark flavours (including the bottom quark) are treated as massless throughout the calculation, except if small masses are needed to regularize a collinear divergence. Since we neglect the small CKM mixing of the third generation with the first two generations, the PDFs of the bottom quark are irrelevant at tree level but enter the result for the QCD bremsstrahlung cross sections (see section 2.3).

In this work, we describe $W + jet$ production up to an accuracy of $\mathcal{O}(\alpha^3 \alpha_s)$. Hence, we also include the $\mathcal{O}(\alpha^3)$ tree-level processes with a photon in the initial state,

$$\mathrm{u}_i \, \gamma \rightarrow \mathrm{W}^+ \mathrm{d}_j \rightarrow l^+ \nu_l \, \mathrm{d}_j \,, \tag{2.5}$$

$$\bar{\mathrm{d}}_j \, \gamma \rightarrow \mathrm{W}^+ \bar{\mathrm{u}}_i \rightarrow l^+ \nu_l \, \bar{\mathrm{u}}_i \,. \tag{2.6}$$

The tree-level Feynman diagrams for process (2.5) are shown in figure 2. The photon content of the proton has been quantified in the MRSTQED2004 PDFs [29]. Since the photon also couples to the charged lepton and the intermediate W boson, the amplitude is more involved than its QCD counterpart. In this work, we do not consider the crossed processes corresponding to $W + \mathrm{photon}$ production. At tree level, $W + jet$ and $W + \mathrm{photon}$ final states can be distinguished trivially, however, at NLO the definition of the $W + jet$ final state has to be done with care when additional photons are present. This issue and our treatment are discussed in detail in section 2.3.

To define the electromagnetic coupling constant α, we use the G_μ scheme, i.e. we derive α from the Fermi constant according to

$$\alpha_{G_\mu} = \frac{\sqrt{2} G_\mu M_\mathrm{W}^2}{\pi} \left(1 - \frac{M_\mathrm{W}^2}{M_\mathrm{Z}^2} \right) . \tag{2.7}$$

In this scheme, the weak corrections to muon decay Δr are included in the charge renormalization constant (see e.g. ref. [9]). As a consequence, the EW corrections are independent

of logarithms of the light-quark masses. Moreover, this definition effectively resums the contributions associated with the running of α from zero to the W-boson mass and absorbs leading universal corrections $\propto G_\mu m_t^2$ from the ρ parameter into the LO amplitude.

For corrections due to collinear final-state radiation it would be more appropriate to use $\alpha(0)$ defined in the Thomson limit to describe the corresponding coupling. On the other hand, using α_{G_μ} everywhere is best suited to describe the large corrections due to Sudakov logarithms in the high-energy regime. Thus, the optimal choice cannot be achieved in one particular input scheme and necessarily requires more refinements. In particular, among other things, higher-order effects from multi-photon emission should also be included at this level of precision which is beyond the scope of this work. The difference of the two schemes only amounts to about 3% of the EW corrections.

We employ the traditional Feynman-diagrammatic approach to calculate all relevant amplitudes in the 't Hooft-Feynman gauge. For a numerical evaluation at the amplitude level we use the Weyl-van-der-Waerden spinor formalism. To ensure the correctness of the presented results we have performed two independent calculations which are in mutual agreement.

One calculation starts from diagrammatic expressions for the one-loop corrections generated by FEYNARTS 1.0 [30]. The algebraic evaluation of the loop amplitudes is performed with an in-house program written in *Mathematica*, and the results are automatically transferred to *Fortran*. The Born and bremsstrahlung amplitudes are calculated and optimised by hand and directly included into a *Fortran* program for numerical evaluation. A specific parametrization of phase space is used for an adaptive Monte Carlo integration employing the VEGAS [31] algorithm.

The second calculation is based on FEYNARTS 3.2 [32] and FORMCALC version 3.1 [33]. The translation of the amplitudes into the Weyl-van-der-Waerden formalism as presented in ref. [34] is performed with the program POLE [35]. POLE also provides an interface to the multi-channel phase-space integrator LUSIFER [36] which has been extended to use VEGAS [31] in order to optimise each phase-space mapping.

2.2 Virtual corrections

We calculate the virtual one-loop QCD and EW corrections for the partonic processes (2.1)–(2.3) to order $\mathcal{O}(\alpha^2\alpha_s^2)$ and $\mathcal{O}(\alpha^3\alpha_s)$, respectively. Since the partonic processes (2.5) and (2.6) are already suppressed by α/α_s at LO, we only need to include the NLO QCD corrections for these channels to reach the required accuracy. The QCD corrections are straight-forward to implement and are induced by self-energy, vertex, and box (4-point) diagrams only. The NLO EW corrections are more involved and include pentagon (5-point) diagrams. There are $\mathcal{O}(100)$ diagrams per partonic channel, including 6 pentagons and 20 boxes. The generic structure of the contributing diagrams is indicated in figure 3, and the pentagon diagrams are explicitly given in figure 4. The different channels are related by crossing symmetry.

The potentially resonant W bosons require a proper inclusion of the finite gauge-boson width in the propagators. We use the complex-mass scheme, which was introduced in ref. [26] for LO calculations and generalized to the one-loop level in ref. [27]. In this

Self-energy insertions:
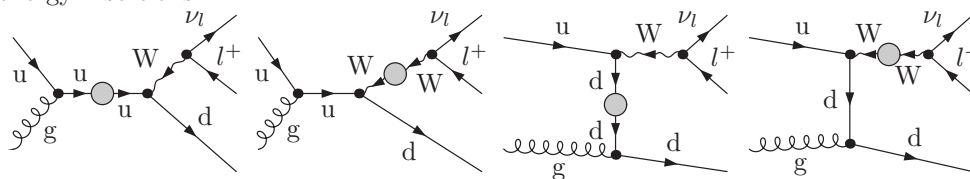
Triangle insertions:
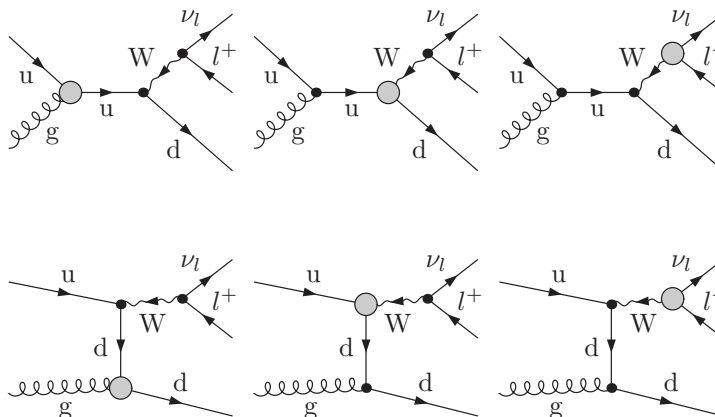
Box and pentagon insertions:
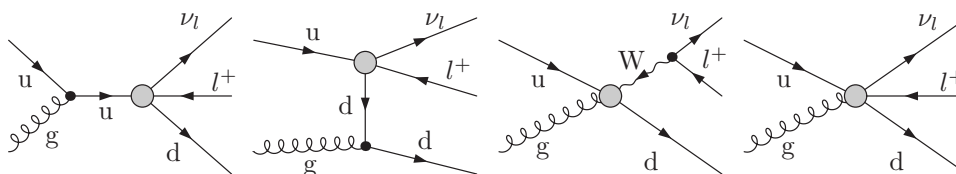
Figure 3. Contributions of different one-particle irreducible vertex functions (indicated as blobs) to the LO process (2.2); there are contributions from self-energies, triangles, boxes, and pentagon graphs.
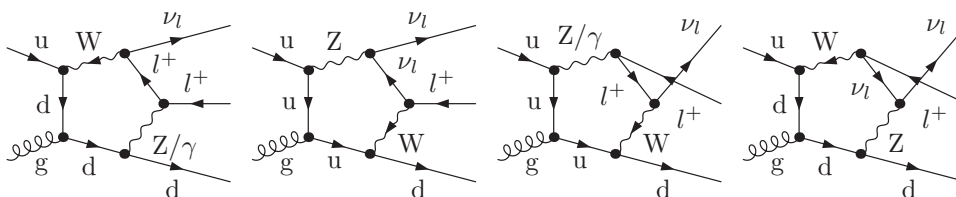
Figure 4. Virtual pentagon contributions to the process (2.2).

approach the W- and Z-boson masses are consistently considered as complex quantities, defined as the locations of the propagator poles in the complex plane. This leads to complex couplings and, in particular, a complex weak mixing angle. The scheme fully respects all relations that follow from gauge invariance. A brief description of the complex-mass scheme can also be found in ref. [37].

The amplitudes can be expressed in terms of standard matrix elements and coefficients, which contain the tensor integrals (following the ideas in the appendix of ref. [38]).

The tensor integrals are recursively reduced to master integrals at the numerical level. The standard scalar integrals are evaluated for complex masses based on the methods and results of ref. [39] using two independent *Fortran* implementations which are in mutual agreement. Results for different regularization schemes are translated into each other with the method of ref. [40]. Tensor and scalar 5-point functions are directly expressed in terms of 4-point integrals [41–43]. Tensor 4-point and 3-point integrals are reduced to scalar integrals with the Passarino-Veltman algorithm [44]. Although we already find sufficient numerical stability with this procedure, we apply the dedicated expansion methods of ref. [43] in exceptional phase-space regions where small Gram determinants appear.

UV divergences are regularized dimensionally. For the infrared (IR), i.e. soft or collinear, divergences we either use pure dimensional regularization with massless gluons, photons, and fermions (except for the top quark), or pure mass regularization with infinitesimal photon, gluon, and small fermion masses, which are only kept in the mass-singular logarithms. When using dimensional regularization, the rational terms of IR origin are treated as described in appendix A of ref. [45].

We use an on-shell renormalization prescription for the EW part of the SM as detailed in ref. [27] for the complex-mass scheme. Employing the G_μ scheme for the definition of the fine-structure constant, we include Δr in the charge renormalization constant as mentioned above. The strong coupling constant is renormalized in the $\overline{\text{MS}}$ scheme with five active flavours. Hence, bottom quarks are included everywhere in the calculation as a massless quark flavour.

2.3 Real corrections

The evaluation of the real corrections has to be done with particular care, both for theoretical consistency as well as to match the experimental observables as closely as possible. Let us first focus on the EW real corrections to the partonic processes (2.1) to (2.3). The emission of an additional photon leads to the processes

$$\text{u}_i \, \bar{\text{d}}_j \rightarrow l^+ \nu_l \, \text{g} \, \gamma \,, \tag{2.8}$$

$$\text{u}_i \, \text{g} \, \rightarrow l^+ \nu_l \, \text{d}_j \, \gamma \,, \tag{2.9}$$

$$\bar{\text{d}}_j \, \text{g} \, \rightarrow l^+ \nu_l \, \bar{\text{u}}_i \, \gamma \,. \tag{2.10}$$

The Feynman diagrams contributing to the process (2.9) are shown in figure 5. Due to the emission of soft photons the real corrections include soft singularities which are cancelled by the virtual corrections independently of the details of the event selection or recombination procedure. If the photon and the charged leptons/quarks are recombined into a pseudo-particle (mimicking the start of hadronic or electromagnetic showers) to form IR-safe observables, all the remaining singularities arising from collinear photon emission in the final state also cancel against the corresponding singularities in the virtual corrections. This requires that all the selection cuts for a given observable are blind to the distribution of momenta in collinear lepton-photon configurations. The left-over collinear singularities due to collinear photon emission off the initial-state quarks are absorbed by a redefinition of the PDFs. Technically, we use the dipole subtraction formalism as specified for photon
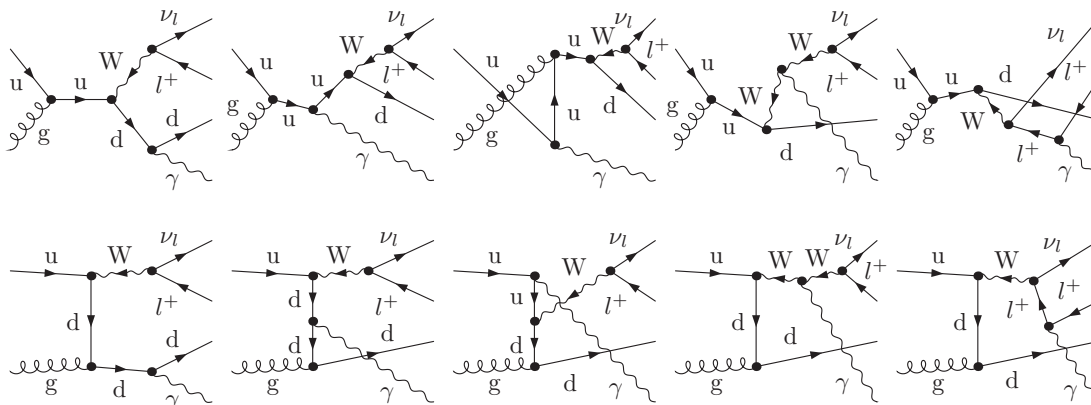
Figure 5. Real photonic bremsstrahlung corrections to the LO process (2.2).

emission in refs. [46, 47] to isolate all the divergences and observe the numerical cancellation. Note that the MRSTQED2004 PDFs, which properly account for all QED effects, are defined in the DIS scheme with respect to QED corrections, as explained in ref. [48].

For muons in the final state it is, however, experimentally possible to separate collinear photons from the lepton, i.e. to observe so-called "bare" muons. Hence, the resulting cross sections are not collinear safe (i.e. the KLN theorem [49] does not apply), and the corresponding collinear singularities show up as logarithms of the small lepton (muon) mass. The lepton mass cuts off the collinear divergence in a physically meaningful way.

In this work, we employ the extension [47] of the subtraction formalism [46], which allows one to calculate cross sections for bare leptons, i.e. cross sections defined without any photon recombination. Like in the standard subtraction formalism, it is sufficient to calculate the real-emission matrix elements for the partonic processes in the massless-fermion approximation. The main difference between the subtraction variants of refs. [46] and [47] concerns the implementation of phase-space cuts. In the standard subtraction formalism [46] it is always assumed that the complete momentum of the lepton and a collinear photon is subject to cuts (as it would be the case after recombination), while the generalization [47] allows for non-collinear-safe cuts that resolve the distribution of the momenta in collinear photon-lepton configurations. This more general cut procedure in the non-collinear-safe case has to be carefully implemented both in the real emission part and the corresponding subtraction terms, in order to ensure the numerical cancellation of singularities. Of course, the treatment of non-collinear-safe cuts leads to a modification of the readded subtraction part as well. In the formulation of ref. [47] this modification assumes the form of an additional (+)-distribution which contains the surviving mass singularity. This (+)-distribution integrates to zero for collinear-safe observables so that the formalism reduces to the well-known standard subtraction formalism. For non-collinear-safe observables the additional logarithms of the lepton mass in the final result are, thus, isolated analytically. For a complete and detailed description of this more general subtraction formalism we refer the reader to ref. [47]. In the following we briefly outline how the logarithms of the lepton mass for our specific example of bare muons in W + jet can be

extracted. We have also used the two-cutoff phase-space slicing to check the results for the EW corrections.

The logarithmically enhanced terms can be directly extracted from the readded integrated subtraction terms. For a final-state emitter and a final-state spectator they can be cast into the form [see (2.14) in ref. [47]]

$$
\int d\Phi_1 \, |\mathcal{M}_{\text{sub},ij}(\Phi_1)|^2 = -\frac{\alpha}{2\pi} Q_i \sigma_i Q_j \sigma_j \int d\tilde{\Phi}_{0,ij} \int_0^1 dz
$$
$$
\times \left\{ G_{ij}^{(\text{sub})}(P_{ij}^2)\delta(1-z) + \left[\bar{\mathcal{G}}_{ij}^{(\text{sub})}(P_{ij}^2,z) \right]_+ \right\}
$$
$$
\times |\mathcal{M}_0(\tilde{p}_i,\tilde{p}_j)|^2 \, \Theta_{\text{cut}}\Big(p_i = z\tilde{p}_i, k = (1-z)\tilde{p}_i, \tilde{p}_j, \{k_n\} \Big), \quad (2.11)
$$

where $Q_{i,j}$ are the fermion charges of emitter i and spectator j, $\tilde{p}_{i,j}$ the momenta, and $\sigma_{i,j} = \pm 1$ correspond to the charge flow [$\sigma_{i,j} = +1(-1)$ for incoming (outgoing) fermions and outgoing (incoming) antifermions]. We denote the LO matrix element by $\mathcal{M}_0(\tilde{p}_i,\tilde{p}_j)$, and $d\tilde{\Phi}_{0,ij}$ indicates the integration over the LO phase space. The cuts on the phase space are implemented via the theta function Θ_{cut} which is zero if a momentum configuration does not pass the cut and one otherwise. Note that Θ_{cut} is a function of $p_i = z\tilde{p}_i$, the photon momentum $k = (1-z)\tilde{p}_i$, and all other momenta, i.e. the momenta of the emitter and the photon after emission are reconstructed from the recombined momentum $\tilde{p}_i$. Here, collinear safety is not guaranteed. The result is indeed presented in a form, where the endpoint contribution $G_{ij}^{(\text{sub})}$, known from the collinear-safe subtraction formalism [46], is explicitly extracted. The term $G_{ij}^{(\text{sub})}$ contains all the fermion and photon mass logarithms that are cancelled by the virtual corrections in mass regularization. The delta-function $\delta(1-z)$ guarantees that this result is unchanged no matter if the cuts are collinear safe or not. As mentioned above, the additional contribution $\bar{\mathcal{G}}_{ij}^{(\text{sub})}$ integrates trivially to zero if the cuts do not depend on z due to the $(+)$-distribution with respect to the z integration. However, there is an additional contribution for non-collinear-safe cuts. For $\bar{\mathcal{G}}_{ij}^{(\text{sub})}$, one finds [47]

$$
\bar{\mathcal{G}}_{ij}^{(\text{sub})}(P_{ij}^2,z) = P_{ff}(z)\left[\ln\left(\frac{P_{ij}^2 z}{m_i^2}\right) - 1\right] + (1+z)\ln(1-z) + 1 - z, \quad (2.12)
$$

where $P_{ij}^2 = (\tilde{p}_i + \tilde{p}_j)^2$ and the splitting function reads

$$
P_{ff}(z) = \frac{1+z^2}{1-z}. \quad (2.13)
$$

This contribution contains the logarithmic contributions we are after. Omitting non-logarithmic terms we find for a particular emitter-spectator contribution

$$
\int d\Phi_1 \, |\mathcal{M}_{\text{sub},ij}(\Phi_1)|^2 = \frac{\alpha}{2\pi} \int d\tilde{\Phi}_{0,ij} \int_0^1 dz \, \Gamma_{ij}(z)|\mathcal{M}_0(\tilde{p}_i,\tilde{p}_j)|^2
$$
$$
\times \left[\Theta_{\text{cut}}\Big(p_i = z\tilde{p}_i, k = (1-z)\tilde{p}_i, \tilde{p}_j, \{k_n\} \Big) - \Theta_{\text{cut}}\Big(p_i = \tilde{p}_i, k = 0, \tilde{p}_j, \{k_n\} \Big) \right]
$$
$$
+ \text{non-singular terms}, \quad (2.14)
$$

where the $(+)$-distribution has been made explicit and we have defined the function

$$\Gamma_{ij}(z) = -Q_i\sigma_i Q_j\sigma_j P_{ff}(z) \ln\left(\frac{P_{ij}^2 z}{m_i^2}\right). \tag{2.15}$$

For an initial-state spectator a, the contribution looks exactly the same, apart from the replacement $P_{ij}^2 \rightarrow -P_{ia}^2$. Using charge conservation $(\sum_j \sigma_j Q_j + \sum_a \sigma_a Q_a = -\sigma_i Q_i)$, one finds for the sum of all subtraction terms corresponding to the emission by a final-state fermion

$$\Gamma_i(z) = \sum_k \Gamma_{ik}(z) = Q_i^2\, P_{ff}(z)\, \ln\left(\frac{Q^2}{m_i^2}\right) - \sum_k Q_i\sigma_i Q_k\sigma_k P_{ff}(z)\ln\left(\frac{|P_{ik}^2|z}{Q^2}\right), \tag{2.16}$$

where k runs over all initial-state and final-state spectators, and we have introduced the scale Q to combine logarithms of the fermion masses. The first term is exactly the first-order leading-logarithmic result in the structure-function approach to final-state radiation [50] (see also ref. [14] for a specific application to W-boson production). In the structure-function approach, Q is interpreted as a factorization scale. Evidently, in our complete $\mathcal{O}(\alpha)$ calculation this scale dependence is absent. Moreover, for real emission events, the full kinematics of the lepton-photon splitting is contained in the calculation, i.e. we are not restricted to the strict collinear limit. For integrated W + jet cross sections, the above result implies an additional negative correction, since we demand a minimum transverse momentum for the charged leptons. Hence, the cut condition in the first theta-function of (2.14) is more restrictive. For distributions, logarithmically enhanced corrections that would contribute to a given transverse-momentum bin with recombination are now shifted to a bin corresponding to $z\tilde{p}_i$ which has, of course, less $p_{\rm T}$ than $\tilde{p}_i$.

Photons and QCD partons always have to be recombined into a single jet if they are sufficiently collinear. This leads to collinear-safe observables if the selection cuts respect the recombination procedure. However, the recombination induces a problem for subprocess (2.8). If the photon and the gluon are accidentally collinear (of course there is no collinear enhancement for these configurations) arbitrarily soft gluons can still pass the jet selection due to a collinear photon. There is a soft-gluon divergence induced by this simple recombination procedure that would be cancelled by the virtual QCD corrections to W + photon production, as e.g. worked out in ref. [23]. To avoid the singularity, one has to distinguish W + photon and W + jet production by means of a more precise event definition employing a cut on the maximal energy or transverse momentum fraction of a photon inside a given jet. However, this procedure spoils the collinear safety of the event definition in subprocesses (2.9) and (2.10). Using again the subtraction formalism [47] to extract the problematic collinear terms, the appearance of an unphysical quark-mass logarithm in the final result signals the necessity to include non-perturbative physics to properly describe the emission of a photon by a quark for exclusive final states. Using dimensional regularisation, the quark-mass logarithm translates into a collinear $1/\epsilon$ pole in the final results, where ϵ quantifies the deviation from the four-dimensionality of space-time. Fortunately, the non-perturbative contribution to the class of events we want to exclude has been measured at LEP in photon+jet events. In these events a photon carries almost all the energy

of a radiating quark in a hadronic Z-boson decay. The relevant collinear physics can be factorized from the underlying hard process and can be cast into a process-independent quark-to-photon fragmentation function $D_{q \to \gamma}(z_\gamma)$, where z_γ is the energy fraction of the photon in the collinear quark-photon configuration.

In analogy to the absorption of initial-state collinear singularities into PDFs, the perturbative singularity can be absorbed into an NLO definition of the fragmentation function [51]. However, in contrast to the PDF analogue, the LO fragmentation function vanishes. Using dimensional regularization (DR) and the $\overline{\text{MS}}$ factorization scheme, one finds

$$D_{q \to \gamma}^{\text{DR}}(z_\gamma) = \frac{\alpha Q_q^2}{2\pi} P_{q \to \gamma}(z_\gamma) \left(\frac{(4\pi)^\epsilon}{\Gamma(1-\epsilon)} \frac{1}{\epsilon} + \ln \frac{\mu^2}{\mu_{\text{F}}^2} \right) + D_{q \to \gamma}^{\text{ALEPH},\overline{\text{MS}}}(z_\gamma, \mu_{\text{F}}), \qquad (2.17)$$

where $D = 4 - 2\epsilon$ is the dimension of space-time, μ is the arbitrary reference mass of dimensional regularization, μ_{F} is the factorization scale for the fragmentation process, and the quark-to-photon splitting function is given by

$$P_{q \to \gamma}(z_\gamma) = \frac{1 + (1 - z_\gamma)^2}{z_\gamma}. \qquad (2.18)$$

Translating the $\overline{\text{MS}}$ definition into the mass regularization (MR) scheme we find

$$D_{q \to \gamma}^{\text{MR}}(z_\gamma) = \frac{\alpha Q_q^2}{2\pi} P_{q \to \gamma}(z_\gamma) \left(\ln \frac{m_q^2}{\mu_{\text{F}}^2} + 2 \ln z_\gamma + 1 \right) + D_{q \to \gamma}^{\text{ALEPH},\overline{\text{MS}}}(z_\gamma, \mu_{\text{F}}). \qquad (2.19)$$

As indicated by the superscript, we will employ the parametrization of the fragmentation function used by the ALEPH collaboration to fit the data [28],

$$D_{q \to \gamma}^{\text{ALEPH},\overline{\text{MS}}}(z_\gamma, \mu_{\text{F}}) = \frac{\alpha Q_q^2}{2\pi} \left(P_{q \to \gamma}(z_\gamma) \ln \frac{\mu_{\text{F}}^2}{(1 - z_\gamma)^2 \mu_0^2} + C \right). \qquad (2.20)$$

Here, the constants μ_0^2 and C are fit parameters and the dependence of the complete fragmentation function on the factorization scale μ_{F} cancels by construction. We use the result of a one-parameter fit where C is constraint to $C = -1 - \ln(M_Z^2/(2\mu_0^2))$ resulting in

$$\mu_0 = 0.14\,\text{GeV} \quad \text{and} \quad C = -13.26\,. \qquad (2.21)$$

Note that we are interested in the fragmentation function to subtract the non-perturbative part of the perturbatively well-defined inclusive (collinear-safe) cross section in which the photon-energy fraction z_γ becomes large[1]. Hence, we are not sensitive to the soft-photon pole of the splitting function for $z_\gamma \to 0$. We convolute the fragmentation function (2.19) with the LO cross section if z_γ is larger than a given cutoff. The result is subtracted from the inclusive result together with the perturbative parts, captured by the subtraction formalism, and the unphysical dependence of the cross section on the quark mass disappears.

---

[1] In contrast, if one did not recombine photons and partons at all to avoid the soft-gluon pole the result would be sensitive to non-perturbative collinear physics, more precisely to the fragmentation function in the whole range of z_γ, in particular for small z_γ where the fragmentation function has not been measured.

The real corrections due to NLO QCD are less subtle. Additional gluon emission and application of crossing symmetry leads to the processes

$$u_i \, \bar{d}_j \rightarrow l^+ \nu_l \, g \, g \,, \tag{2.22}$$

$$u_i \, g \rightarrow l^+ \nu_l \, d_j \, g \,, \tag{2.23}$$

$$\bar{d}_j \, g \rightarrow l^+ \nu_l \, \bar{u}_i \, g \,, \tag{2.24}$$

$$g \, g \rightarrow l^+ \nu_l \, \bar{u}_i \, d_j \,, \tag{2.25}$$

and the external gluon present at LO may also split into two quarks, inducing the processes

$$u_i \, \bar{d}_j \rightarrow l^+ \nu_l \, q_k \, \bar{q}_k \,, \tag{2.26}$$

$$\bar{q}_k \, \bar{d}_j \rightarrow l^+ \nu_l \, \bar{u}_i \, \bar{q}_k \,, \tag{2.27}$$

$$q_k \, \bar{d}_j \rightarrow l^+ \nu_l \, q_k \, \bar{u}_i \quad (q_k \neq u_i, q_k \neq d_j) \,, \tag{2.28}$$

$$u_i \, \bar{q}_k \rightarrow l^+ \nu_l \, d_j \, \bar{q}_k \quad (\bar{q}_k \neq \bar{d}_j, \bar{q}_k \neq \bar{u}_i) \,, \tag{2.29}$$

$$u_i \, q_k \rightarrow l^+ \nu_l \, q_k \, d_j \,, \tag{2.30}$$

$$q_k \, \bar{q}_k \rightarrow l^+ \nu_l \, \bar{u}_i \, d_j \,, \tag{2.31}$$

where q_k stands for up-type quarks u_k with $k = 1, 2$ or for down-type quarks d_k with $k = 1, 2, 3$. Note that the Feynman diagrams are different in the two cases $i = k$ ($j = k$) and $i \neq k$ ($j \neq k$). Taking this difference into account, the remaining sums over flavour can again efficiently be performed when convoluting the squared matrix elements with PDFs. As in the EW case, we use the dipole subtraction method [52] to extract the IR singularities analytically from the numerical phase-space integration. Absorbing all the collinear singularities due to initial-state splittings into the relevant PDFs, the remaining collinear and soft divergences cancel all the divergences of the one-loop QCD corrections for processes (2.1)–(2.3). Here, also the bottom-quark PDF enters the NLO prediction. For example a bottom quark from a proton can emit a gluon which subsequently takes part in the hard process.

Turning to the photon-induced processes, the corresponding bremsstrahlung processes are

$$u_i \, \gamma \rightarrow l^+ \nu_l \, d_j \, g \,, \tag{2.32}$$

$$\bar{d}_j \, \gamma \rightarrow l^+ \nu_l \, \bar{u}_i \, g \,, \tag{2.33}$$

$$g \, \gamma \rightarrow l^+ \nu_l \, \bar{u}_i \, d_j \,. \tag{2.34}$$

All singularities cancel those in the virtual NLO QCD corrections or are absorbed into PDFs.

There is yet another class of corrections contributing at $\mathcal{O}(\alpha^3 \alpha_s)$. For the six-fermion processes (2.26)–(2.31) with two identical quarks, diagrams with gluon exchange can interfere with purely EW diagrams. Exemplarily, the relevant diagrams for one of the contributing subprocesses are shown in figure 6. The result is non-singular due to the restrictions from colour flow, but only if all fermions are distinct the interference contribution vanishes. We have also included these corrections in our calculation. However, their effect turns out

a) $\mathcal{M}^s_{\mathrm{EW}}$:

b) $\mathcal{M}^t_{\mathrm{QCD}}$:

c) $\mathcal{M}_{\mathrm{QCD}}\mathcal{M}^*_{\mathrm{EW}}$:

$$\mathcal{M}^t_{\mathrm{QCD}}(\mathcal{M}^s_{\mathrm{EW}})^* \propto \mathrm{Tr}[T^a T^a]$$
$\rightarrow$ interference non zero

$$\mathcal{M}^s_{\mathrm{QCD}}(\mathcal{M}^s_{\mathrm{EW}})^* \propto (\mathrm{Tr}[T^a])^2$$
$\rightarrow$ interference vanishes
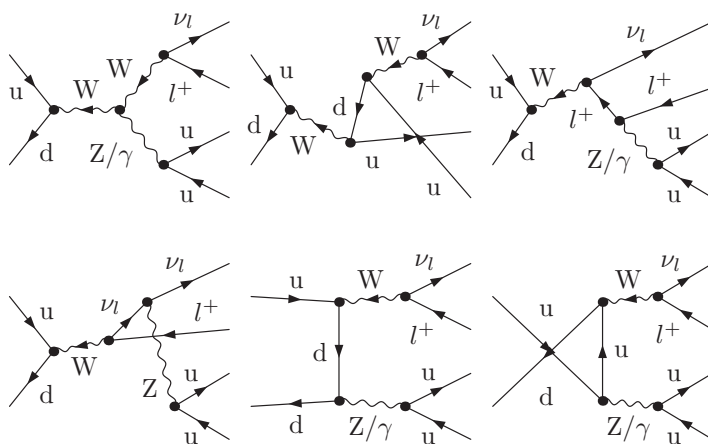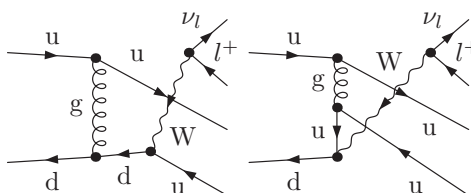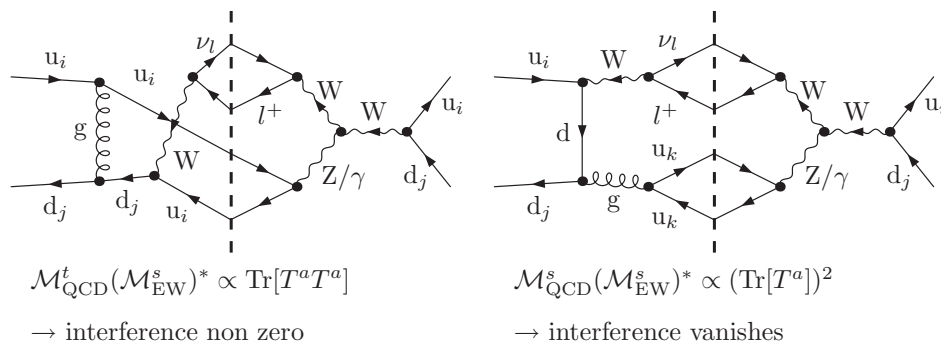
Figure 6. The interference between EW and QCD diagrams: a) EW diagrams with s-channel-like colour flow for process (2.26) with $q_k = \mathrm{u}_k$. b) QCD diagrams with t-channel-like colour flow. c) EW and QCD diagrams of both s- or t-type do not contribute (right). However, for $i = k$, there is an interference contribution from diagrams of different types that is non-zero. The full interference term for the partonic process (2.26) reads $2\,\mathrm{Re}[\mathcal{M}^t_{\mathrm{QCD}}(\mathcal{M}^s_{\mathrm{EW}})^* + \mathcal{M}^s_{\mathrm{QCD}}(\mathcal{M}^t_{\mathrm{EW}})^*]$. All other partonic interference contributions with the same flavour structure can be obtained by applying the same crossing procedure to $\mathcal{M}^{s/t}_{\mathrm{QCD}}$ and $\mathcal{M}^{s/t}_{\mathrm{EW}}$.

to be phenomenologically negligible. Diagrams with an internal top propagator and two W bosons do not contribute if mixing with quarks of the third generation is neglected.

– 13 –

3 Numerical results

3.1 Input parameters and setup

The relevant SM input parameters are

$$
\begin{aligned}
G_\mu &= 1.16637 \times 10^{-5}\,\text{GeV}^{-2}, & \Lambda_{\text{QCD}} &= 239\,\text{MeV}, & \alpha_{\text{s}}(M_Z) &= 0.11899, \\
M_W^{\text{OS}} &= 80.398\,\text{GeV}, & \Gamma_W^{\text{OS}} &= 2.141\,\text{GeV}, \\
M_Z^{\text{OS}} &= 91.1876\,\text{GeV}, & \Gamma_Z^{\text{OS}} &= 2.4952\,\text{GeV}, & M_H &= 120\,\text{GeV}, \\
m_{\text{e}} &= 0.510998910\,\text{MeV}, & m_\mu &= 105.658367\,\text{MeV}, & m_{\text{t}} &= 172.6\,\text{GeV}, \\
|V_{\text{ud}}| &= |V_{\text{cs}}| = 0.974, & |V_{\text{us}}| &= |V_{\text{cd}}| = \sqrt{1 - |V_{\text{cs}}|^2},
\end{aligned}
\tag{3.1}
$$

which essentially follow ref. [53]. The CKM matrix is included via global factors in the partonic cross sections for the different possible quark flavours. Within loops the CKM matrix is set to unity, because its effect is negligible there.

Using the complex-mass scheme [27], we employ a fixed width in the resonant W- and Z-boson propagators in contrast to the approach used at LEP and Tevatron to fit the W and Z resonances, where running widths are taken. Therefore, we have to convert the "on-shell" (OS) values of M_V^{OS} and Γ_V^{OS} ($V = $ W, Z), resulting from LEP and Tevatron, to the "pole values" denoted by M_V and Γ_V. The relation between the two sets of values is given by [54]

$$
M_V = M_V^{\text{OS}}/\sqrt{1 + (\Gamma_V^{\text{OS}}/M_V^{\text{OS}})^2}, \qquad \Gamma_V = \Gamma_V^{\text{OS}}/\sqrt{1 + (\Gamma_V^{\text{OS}}/M_V^{\text{OS}})^2}, \tag{3.2}
$$

leading to

$$
\begin{aligned}
M_W &= 80.370\dots\,\text{GeV}, & \Gamma_W &= 2.1402\dots\,\text{GeV}, \\
M_Z &= 91.153\dots\,\text{GeV}, & \Gamma_Z &= 2.4943\dots\,\text{GeV}.
\end{aligned}
\tag{3.3}
$$

We make use of these mass and width parameters in the numerics discussed below, although the difference between using M_V or M_V^{OS} would be hardly visible.

As explained in section 2.1, we adopt the G_μ scheme, where the electromagnetic coupling α is set to α_{G_μ}. In this scheme the electric-charge renormalization constant does not contain logarithms of the light-fermion masses, in contrast to the $\alpha(0)$ scheme, so that the results become practically independent of the light-quark masses.

The $\mathcal{O}(\alpha)$-improved MRSTQED2004 set of PDFs [29] is used throughout implying the value of $\alpha_{\text{s}}(M_Z)$ stated in (3.1). We use standard two-loop running of the strong coupling constant in the 5-flavour scheme with $\Lambda_{\text{QCD}} = 239\,\text{MeV}$. Since the MRSTQED2004 PDF set has been released, there have been considerable improvements for PDFs, in particular with respect to the heavy-flavour treatment. Since recent PDF sets do not include QED effects we stick to MRSTQED2004 for theoretical consistency. Hence, all the absolute values for cross sections lack the recent PDF improvements. However, the presented relative corrections should be more stable with respect to variations in the PDFs than absolute predictions.

The QCD and QED factorization scales as well as the renormalization scale are always identified. For low-p_{T} jets, the scale of the process is given by the invariant mass of the

leptons which in turn peaks around M_{W} for resonant W-boson production. Hence, one natural choice is the W-boson mass, i.e. $\mu_{\mathrm{R}} = \mu_{\mathrm{F}} = M_{\mathrm{W}}$. For high-$p_{\mathrm{T}}$ jets, well beyond the W-boson scale, however, the relevant scale is certainly larger, and the QCD emission from the initial state is best modelled by the p_{T} of the jet itself (see e.g. ref. [55]). To interpolate between the two regimes, we alternatively use

$$\mu = \mu_{\mathrm{R}} = \mu_{\mathrm{F}} = \sqrt{M_{\mathrm{W}}^2 + (p_{\mathrm{T}}^{\mathrm{had}})^2}\,, \tag{3.4}$$

where $p_{\mathrm{T}}^{\mathrm{had}}$ is given by the p_{T} of the summed four-momenta of all partons, i.e. quarks and/or gluons in the final state. At LO, $p_{\mathrm{T}}^{\mathrm{had}}$ is simply the p_{T} of the one final-state jet. We present results for both scale choices.

3.2 Phase-space cuts and event selection

In order to define IR-safe observables for the process $\mathrm{pp/p\bar{p}} \to \mathrm{W}^+ + \mathrm{jet} \to l^+ \nu_l + \mathrm{jet} + X$ we recombine final-state partons and photons to pseudo-particles and impose a set of phase-space cuts as detailed in the following subsections.

3.2.1 Recombination

To define the recombination procedure and the separation cuts, we use the variables $R_{ij} = \sqrt{(y_i - y_j)^2 + \phi_{ij}^2}$, where y_i denotes the rapidity $y = \frac{1}{2}\ln[(E + p_{\mathrm{L}})/(E - p_{\mathrm{L}})]$ of particle i and ϕ_{ij} is the azimuthal angle in the transverse plane between the particles i and j. In the definition of the rapidity, E denotes the particle's energy and p_{L} the momentum along the beam axis. The recombination procedure, where we simply add four-momenta to form a pseudo-particle, works as follows:

1. For observables with bare muons we do not recombine photons and leptons. For inclusive observables, a photon and a lepton are recombined for $R_{\gamma l} < 0.1$.

2. A photon and a parton a (quark or gluon) are recombined for $R_{\gamma a} < 0.5$. In this case, we use the energy fraction of the photon inside the jet, $z_{\gamma} = E_{\gamma}/(E_{\gamma} + E_a)$, to distinguish between W + jet and W + γ production. If $z_{\gamma} > 0.7$, the event is regarded as a part of W + γ production and rejected because it lacks any other hard jet at NLO. This event definition is not collinear safe and requires the use of quark-to-photon fragmentation functions to include the non-perturbative part of the quark-photon splitting as explained in section 2.3. Our results are not very sensitive to the specific choice of the cut on z_{γ}.

3. Two partons a, b are recombined for $R_{ab} < 0.5$. For our simple final-state configurations, this procedure is equivalent to the Tevatron Run II k_{T}-algorithm [56] for jet reconstruction with resolution parameter $D = 0.5$.

Technically, we perform a possible photon-lepton recombination before the photon-parton recombination. This procedure is IR safe because the triple-soft/collinear situation that a photon should have been first recombined with a parton, but was erroneously first recombined with a lepton, is excluded by our basic cuts.

3.2.2 Basic cuts

After applying the recombination procedure of the previous section we define W+jet events by the following basic cuts:

1. A partonic object (after a possible recombination) is called a jet if its transverse momentum p_T is larger than $p_{T,jet}^{cut} = 25\,\text{GeV}$. Events are required to include at least one jet.

2. We demand a charged lepton with transverse momentum $p_{T,l} > 25$ GeV and a missing momentum $\not{p}_T > 25$ GeV.

3. The events have to be central, i.e. the lepton and at least one jet have to be produced in the rapidity range $|y| < y_{max} = 2.5$.

4. The lepton has to be isolated, i.e. the event is discarded if the distance between the lepton and a jet $R_{l\text{jet}}$ is smaller than 0.5.
   The lepton-jet separation is also required for jets with $|y| > y_{max}$. It is important to exclude low-p_T partons from the lepton-jet separation procedure (guaranteed by step 1.), since otherwise observables would not be IR safe.

While the EW corrections differ for final-state electrons and muons without photon recombination, the corrections become universal in the presence of photon recombination, since the lepton-mass logarithms cancel in this case, in accordance with the KLN theorem. Numerical results are presented for photon recombination and for bare muons.

For certain observables, we apply a jet veto against a second hard jet. To be specific, we veto any sub-leading jet with $p_T > p_{T,j_1}/2$, where p_{T,j_1} denotes the p_T of the "leading" jet, i.e. the one with maximal p_T.

3.3 Results on cross sections

We first consider W^+ production in association with a jet at the LHC, i.e. a pp initial state with a centre-of-mass (CM) energy of $\sqrt{s} = 14\,\text{TeV}$.

We present the LO cross section σ_0 and various types of corrections δ, defined relative to the LO cross section by $\sigma = \sigma_0 \times (1 + \delta)$. Concerning the EW corrections, we distinguish the cross section $\sigma_{EW}^{\mu^+\nu_\mu}$ for bare muons and σ_{EW}^{rec} for which lepton-photon recombination is employed as defined above. Accordingly, the corresponding corrections are labelled $\delta_{EW}^{\mu^+\nu_\mu}$ and δ_{EW}^{rec}, respectively. An additional label specifies which renormalization and factorization scale is used. Either we use the fixed scale ($\mu = M_W$) or we determine the scale on an event-by-event basis by the kinematical configuration of the final state (var), as specified in (3.4). For the EW corrections the difference is not expected to be large, since the LO and the NLO results depend on the renormalization scale for α_s and the QCD factorization scale in the same way. However, for the QCD part a sensible scale choice can be crucial for the stability of the perturbative series. Accordingly, the QCD corrections are labelled $\delta_{QCD}^{\mu=M_W}$ for a fixed scale choice and δ_{QCD}^{var} for the scale choice defined in (3.4).

As shown below, the QCD corrections become larger and larger with increasing p_T of the leading jet. The increase in the cross section results from a new kinematical configuration which is available for the W + 2 jets final state. The large p_T of the leading jet is not balanced by the leptons, as required at LO, but by the second jet. Hence, we encounter the production of 2 jets where one of the quark lines radiates a relatively soft W boson. This part of the cross section, which does not really correspond to a true NLO correction to W + jet production, can be separated by employing a veto against a second hard jet in real-emission events. Hence, we present NLO QCD corrections with a jet veto, ($\delta_{\mathrm{QCD,veto}}^{\mu=M_{\mathrm{W}}}$, $\delta_{\mathrm{QCD,veto}}^{\mathrm{var}}$), and without a jet veto, ($\delta_{\mathrm{QCD}}^{\mu=M_{\mathrm{W}}}$, $\delta_{\mathrm{QCD}}^{\mathrm{var}}$).

Using a jet veto based on a fixed p_T value for the second jet is not well suited. It will either cut away relatively collinear emission events in the high-p_T tails of the leading-jet distribution (leading to large negative corrections) or it has to be chosen too large to be effective in the intermediate-p_T parts of the distribution. Hence, we veto any sub-leading jet with $p_T > p_{\mathrm{T,j_1}}/2$, where $p_{\mathrm{T,j_1}}$ denotes the p_T of the leading jet. As shown below, this jet veto indeed effectively removes events with back-to-back kinematics.

We also investigate the impact of the photon-induced tree-level processes (2.5) and (2.6) and the corresponding NLO QCD corrections including the real-emission processes (2.32), (2.33), and (2.34). Since even the LO photon-induced cross section is a small effect, we show its relative impact $\delta_{\gamma,\mathrm{Born}}$ with respect to the LO cross section where initial states with photons are not taken into account. Including the NLO QCD corrections, the relative impact of the full NLO cross section is denoted by $\delta_{\gamma,\mathrm{NLO}}$. The impact of the interference contribution introduced at the end of section 2.3 is denoted by δ_{IF}. Additional labels again indicate the scale choice and the usage of a jet veto.

Table 1 shows the LO predictions and the above corrections for different cuts on the p_T of the charged lepton $p_{\mathrm{T},l}$. All other cuts and the corresponding event selection follow our default choice as introduced in section 3.2. All integrated cross sections and, hence, the corrections are dominated by events close to the lowest accepted $p_{\mathrm{T},l}$, as can be seen by the rapid decrease of the integrated cross section when increasing the $p_{\mathrm{T},l}$ cut.

Tables 2 and 3 show the analoguous results for a variation of cuts on the transverse mass of the final-state leptons, defined by

$$M_{\mathrm{T},l\nu_l} = \sqrt{2p_{\mathrm{T},l}\,\not{p}_{\mathrm{T}}(1 - \cos \phi_{l\nu_l})}\,,\tag{3.5}$$

and the p_T of the leading jet $p_{\mathrm{T,jet}}$, respectively. The transverse mass and the $p_{\mathrm{T},l}$ distributions are particularly relevant for the measurement of the W-boson mass at hadron colliders. For this measurement, W-boson events without or with very little additional jet activity are selected. Nevertheless, the calculation of the EW corrections in the presence of an additional jet supplies a handle to quantify how well the interplay of QCD and EW corrections is understood.

Note that for a given $p_{\mathrm{T,jet}}$ both leptons share the recoil since they stem from a boosted W boson and are therefore preferably emitted in the same direction. Accordingly, the LO cross section for a given cut on $p_{\mathrm{T},l}$ is smaller than for the same cut on $p_{\mathrm{T,jet}}$, because on average the required CM energy is larger. In other words, there is a kinematic and

pp → $l^+\nu_l$ jet + X at $\sqrt{s} = 14\,\mathrm{TeV}$						
$p_{\mathrm{T},l}/\,\mathrm{GeV}$	$25-\infty$	$50-\infty$	$100-\infty$	$200-\infty$	$500-\infty$	$1000-\infty$
$\sigma_{\mathrm{Born}}^{\mu=M_{\mathrm{W}}}/\,\mathrm{fb}$	508568(11)	163715(5)	13095.5(4)	1484.16(4)	44.476(1)	1.37894(5)
$\sigma_{\mathrm{Born}}^{\mathrm{var}}/\,\mathrm{fb}$	501826(11)	159482(5)	11481.8(4)	1124.67(3)	25.8791(9)	0.64346(2)
$\delta_{\mathrm{EW}}^{\mu^+\nu_\mu,\mathrm{var}}/\%$	−3.0	−5.4	−9.0	−14.8	−25.8(1)	−36.7(1)
$\delta_{\mathrm{EW}}^{\mathrm{rec},\mathrm{var}}/\%$	−2.2	−3.2	−6.5	−11.7	−21.6(1)	−31.4(1)
$\delta_{\mathrm{QCD}}^{\mu=M_{\mathrm{W}}}/\%$	48.2(1)	34.6(1)	50.9(1)	30.3(1)	−15.9(1)	−60.4(1)
$\delta_{\mathrm{QCD}}^{\mathrm{var}}/\%$	47.9(1)	34.1(1)	54.6(1)	46.2(1)	27.5(1)	6.1(1)
$\delta_{\gamma,\mathrm{Born}}^{\mathrm{var}}/\%$	0.4	0.6	1.7	2.7	4.1(1)	4.9(1)
$\delta_{\gamma,\mathrm{NLO}}^{\mathrm{var}}/\%$	0.4	0.6	1.7	2.6	4.1(1)	5.0(1)
$\delta_{\mathrm{IF}}^{\mathrm{var}}/\%$	0.05	0.02	0.02	0.01	−0.05	−0.1

Table 1. Integrated cross sections for different cuts on the lepton transverse momentum at the LHC. We show the LO results for both a variable and a constant scale. The relative EW corrections δ_{EW} are given with and without lepton-photon recombination. The QCD corrections δ_{QCD} are presented for a fixed as well as a variable scale. The corrections due to photon-induced processes δ_γ, and the contributions from interference terms δ_{IF} are presented for a variable scale. The error from the Monte Carlo integration for the last digit(s) is given in parenthesis as far as significant. See text for details.

pp → $l^+\nu_l$ jet + X at $\sqrt{s} = 14\,\mathrm{TeV}$						
$M_{\mathrm{T},l\nu_l}/\,\mathrm{GeV}$	$50-\infty$	$100-\infty$	$200-\infty$	$500-\infty$	$1000-\infty$	$2000-\infty$
$\sigma_{\mathrm{Born}}^{\mu=M_{\mathrm{W}}}/\,\mathrm{fb}$	450663(10)	7102.5(6)	752.01(2)	53.290(2)	5.0634(1)	0.240331(7)
$\sigma_{\mathrm{Born}}^{\mathrm{var}}/\,\mathrm{fb}$	446072(10)	6937.6(6)	714.64(2)	48.618(1)	4.4510(1)	0.202315(6)
$\delta_{\mathrm{EW}}^{\mu^+\nu_\mu,\mathrm{var}}/\%$	−3.1	−5.2	−8.2	−14.8	−22.5	−33.0(1)
$\delta_{\mathrm{EW}}^{\mathrm{rec},\mathrm{var}}/\%$	−2.2	−3.7	−6.8	−12.8	−19.9	−29.4(1)
$\delta_{\mathrm{QCD}}^{\mu=M_{\mathrm{W}}}/\%$	47.7(1)	30.5(1)	11.7(1)	−15.7(1)	−40.6(1)	−70.0(1)
$\delta_{\mathrm{QCD}}^{\mathrm{var}}/\%$	47.6(1)	31.0(1)	14.4(1)	−8.8(1)	−30.5(1)	−56.0(1)
$\delta_{\gamma,\mathrm{Born}}^{\mathrm{var}}/\%$	0.4	0.3	0.4	0.5	0.4	0.3
$\delta_{\gamma,\mathrm{NLO}}^{\mathrm{var}}/\%$	0.3	0.3	0.4	0.5	0.4	0.3
$\delta_{\mathrm{IF}}^{\mathrm{var}}/\%$	0.1	0.01	−0.05	−0.1	−0.1	−0.1

Table 2. Integrated cross sections for different cuts on the transverse mass of the W at the LHC.

pp $\rightarrow l^+\nu_l$ jet $+ X$ at $\sqrt{s} = 14\,\mathrm{TeV}$						
$p_{\mathrm{T,jet}}/\,\mathrm{GeV}$	$25-\infty$	$50-\infty$	$100-\infty$	$200-\infty$	$500-\infty$	$1000-\infty$
$\sigma_{\mathrm{Born}}^{\mu=M_{\mathrm{W}}}/\,\mathrm{fb}$	508568(11)	182462(4)	49702(1)	8096.3(2)	315.061(5)	11.6750(2)
$\sigma_{\mathrm{Born}}^{\mathrm{var}}/\,\mathrm{fb}$	501826(11)	176106(4)	45313(1)	6488.9(1)	184.742(3)	4.78109(8)
$\delta_{\mathrm{EW}}^{\mu^+\mu_\mu,\mathrm{var}}/\%$	-3.0	-3.3	-4.7	-8.6	-18.1	$-28.4(1)$
$\delta_{\mathrm{EW}}^{\mathrm{rec},\mathrm{var}}/\%$	-2.2	-2.6	-4.2	-8.3	-18.0	$-28.3(1)$
$\delta_{\mathrm{QCD}}^{\mu=M_{\mathrm{W}}}/\%$	48.2(1)	64.7(1)	80.6(1)	115.3(1)	188.8(1)	270.2(1)
$\delta_{\mathrm{QCD}}^{\mathrm{var}}/\%$	47.9(1)	65.5(1)	85.8(1)	135.1(1)	270.3(1)	495.5(1)
$\delta_{\mathrm{QCD,veto}}^{\mu=M_{\mathrm{W}}}/\%$	21.7(1)	18.5(1)	22.5(1)	24.2(1)	5.7(1)	$-26.0(1)$
$\delta_{\mathrm{QCD,veto}}^{\mathrm{var}}/\%$	22.5(1)	21.3(1)	29.9(1)	42.8(1)	52.7(1)	59.5(1)
$\delta_{\gamma,\mathrm{Born}}^{\mathrm{var}}/\%$	0.4	0.7	1.3	2.0	3.4	5.2
$\delta_{\gamma,\mathrm{NLO}}^{\mathrm{var}}/\%$	0.4	0.7	1.2	1.9	3.3	5.2
$\delta_{\gamma,\mathrm{NLO,veto}}^{\mathrm{var}}/\%$	0.3	0.6	1.1	1.8	3.1	4.7
$\delta_{\mathrm{IF}}^{\mathrm{var}}/\%$	0.05	0.1	0.5	1.9	11.5	49.9(1)
$\delta_{\mathrm{IF,veto}}^{\mathrm{var}}/\%$	0.01	0.03	0.1	0.4	1.6	4.7

Table 3. Integrated cross sections for different cuts on the p_{T} of the leading jet at the LHC. Corrections with a second jet in real emission events are shown with and without a jet veto.

an additional PDF suppression of events with a cut on the lepton p_{T} compared to events with the same cut on the jet p_{T}. For large values of $M_{\mathrm{T},l\nu_l}$, the W boson is necessarily produced far off shell so that the cross section is further suppressed. The presented cut values for $M_{\mathrm{T},l\nu_l}$ are chosen because one finds $M_{\mathrm{T},l\nu_l} = 2p_{\mathrm{T},l}$ for back-to-back leptons in the rest frame of the decaying W boson.

For the most inclusive cross section (left columns in table 1 or table 3) the EW corrections are at the percent level and negative. The difference in scale choice is not important, and due to the recombination procedure $\delta_{\mathrm{EW}}^{\mathrm{rec}}$ is slightly smaller in absolute size. With increasing $p_{\mathrm{T},l}$ cut, the relevant CM energies rise, and the well-known Sudakov logarithms in the virtual EW corrections start to dominate the total corrections as expected. For $p_{\mathrm{T},l} > 1000\,\mathrm{GeV}$, the EW corrections reach the level of -30%. This behaviour is generic and also holds true for the cross sections with varying cuts on the transverse mass or $p_{\mathrm{T},\mathrm{jet}}$. We compare the EW corrections for $p_{\mathrm{T},\mathrm{jet}}$ with previous results obtained in an on-shell approximation together with the differential distributions in section 3.4.

Turning to the NLO QCD results, the corrections $\delta_{\mathrm{QCD}}^{\mathrm{var}}$ for different cuts on $p_{\mathrm{T},l}$, as shown in table 1, are sizable and reach the 50% level for intermediate cut values. For low cut values, $\delta_{\mathrm{QCD}}^{\mu=M_{\mathrm{W}}}$ is practically the same. However, for large cut values, the corrections

for a fixed scale differ significantly. Here, $\delta_{\rm QCD}^{\mu=M_{\rm W}}$ grows large and negative to compensate for the overestimated LO cross section, which is larger by more than a factor of two with respect to $\sigma_0^{\rm var}$. This is expected, since the hard jet recoiling against the high-$p_{\rm T}$ lepton should be reflected in the scale choice. Including the NLO QCD corrections, the difference between the results obtained with our two scale choices is significantly reduced.

For small cut values on the transverse mass, as shown in table 2, the corrections are quite similar to the ones of the corresponding cuts on $p_{\rm T,l}$. However, for large $M_{\rm T,l\nu_l}$, both scale choices fail to reflect the kinematical situation, since the production of a far off-shell W boson is dominated by the region near the threshold set by the cut on $M_{\rm T,l\nu_l}$. In this region the W boson decays mainly to back-to-back leptons with relatively soft jet activity. Hence, $\delta_{\rm QCD}^{\mu=M_{\rm W}}$ as well as $\delta_{\rm QCD}^{\rm var}$ become large and negative. A scale choice based on the CM energy of the event or a scale choice reflecting the invariant mass of the lepton pair[2] would be more adequate.

As discussed above, the integrated NLO QCD cross sections for large $p_{\rm T,jet}$ cuts, as shown in table 3, contain large contributions from a completely different class of events for which two jets recoil against each other. Hence, the corrections are huge. The correction $\delta_{\rm QCD}^{\mu=M_{\rm W}}$ is smaller than $\delta_{\rm QCD}^{\rm var}$ because it is defined relative to a larger LO cross section. In absolute size, they are similar. Using the jet veto proposed at the end of section 3.2.2, the corrections are reduced and $\delta_{\rm QCD}^{\rm var}$ rises only to the 50% level for large cut values. The fixed scale choice leads to even smaller corrections $\delta_{\rm QCD}^{\mu=M_{\rm W}}$ in absolute size. However, varying the exact definition of the jet veto, the variable scale turns out to be more robust. We have also verified, that this simple jet veto indeed removes mainly events with back-to-back jets from the event selection. If we only veto events with $\cos\phi_{jj} < -0.99$, where ϕ_{jj} is the azimuthal angle in the transverse plane between the two jets, $\delta_{\rm QCD}^{\rm var}$ for example is still reduced from 495% to 172% for $p_{\rm T,jet} > 1000\,{\rm GeV}$. Events with $\cos\phi_{jj} > 0$ do not have any noticeable effect.

The contribution δ_γ from the photon-induced processes are small and only reach up to 5% for large cuts on $p_{\rm T,l}$ or $p_{\rm T,jet}$ where the EW and QCD corrections to the dominating tree processes are by far larger. The NLO corrections to the photon-induced processes are phenomenologically completely irrelevant.

The corrections due to the interference between EW and QCD diagrams also turn out to be unimportant. They only increase together with the NLO QCD corrections for large $p_{\rm T,jet}$. Once a sensible jet veto is applied, they disappear again.

The qualitative features of the corrections at the Tevatron, where protons and antiprotons collide at $\sqrt{s} = 1.96\,{\rm TeV}$, are very similar to those at the LHC. At the Tevatron the high-energy, Sudakov regime is not as accessible as at the LHC but the onset of the Sudakov dominance is nevertheless visible as can be seen for the different observables in tables 4–6. We have adapted the range for the different integrated cross sections to the kinematic reach of the Tevatron.

---

[2]The scale $\mu = \sqrt{M_{l\nu_l}^2 + (p_{\rm T}^{\rm W})^2}$, where $M_{l\nu_l}$ is the invariant mass of the two leptons in the final state and $p_{\rm T}^{\rm W}$ denotes their transverse momentum, would also be an adequate choice.

$p\bar{p} \rightarrow l^+\nu_l$ jet $+ X$ at $\sqrt{s} = 1.96\,\mathrm{TeV}$						
$p_{\mathrm{T},l}/\,\mathrm{GeV}$	$25 - \infty$	$50 - \infty$	$75 - \infty$	$100 - \infty$	$200 - \infty$	$300 - \infty$
$\sigma_{\mathrm{Born}}^{\mu=M_{\mathrm{W}}}/\,\mathrm{fb}$	37341.5(7)	10560.8(4)	1007.54(4)	263.50(1)	7.2415(4)	0.39000(2)
$\sigma_{\mathrm{Born}}^{\mathrm{var}}/\,\mathrm{fb}$	36056.0(7)	10049.9(4)	863.34(4)	209.484(9)	4.8338(2)	0.23655(1)
$\delta_{\mathrm{EW}}^{\mu^+\nu_\mu,\mathrm{var}}/\%$	-2.8	-5.4	-6.8	-8.2	$-13.2(1)$	$-17.4(1)$
$\delta_{\mathrm{EW}}^{\mathrm{rec},\mathrm{var}}/\%$	-1.9	-2.9	-4.0	$-5.3(1)$	-9.1	-12.4
$\delta_{\mathrm{QCD}}^{\mu=M_{\mathrm{W}}}/\%$	33.5(1)	23.8(1)	27.7(1)	18.3(1)	$-6.4(1)$	$-22.2(1)$
$\delta_{\mathrm{QCD}}^{\mathrm{var}}/\%$	36.3(1)	27.3(1)	40.0(1)	36.8(1)	28.2(1)	21.5(1)
$\delta_{\gamma,\mathrm{Born}}^{\mathrm{var}}/\%$	0.4	0.5	1.2	1.4	1.5	1.3
$\delta_{\gamma,\mathrm{NLO}}^{\mathrm{var}}/\%$	0.4	0.5	1.2	1.4	1.5	1.3
$\delta_{\mathrm{IF}}^{\mathrm{var}}/\%$	-0.1	-0.1	-0.2	-0.2	-0.2	-0.1

Table 4. Integrated cross sections for different cuts on the lepton transverse momentum at the Tevatron.

$p\bar{p} \rightarrow l^+\nu_l$ jet $+ X$ at $\sqrt{s} = 1.96\,\mathrm{TeV}$						
$M_{\mathrm{T},l\nu_l}/\,\mathrm{GeV}$	$50 - \infty$	$100 - \infty$	$150 - \infty$	$200 - \infty$	$400 - \infty$	$600 - \infty$
$\sigma_{\mathrm{Born}}^{\mu=M_{\mathrm{W}}}/\,\mathrm{fb}$	34421.6(6)	434.45(3)	80.338(2)	27.5868(9)	1.25355(4)	0.088241(3)
$\sigma_{\mathrm{Born}}^{\mathrm{var}}/\,\mathrm{fb}$	33359.8(6)	415.57(3)	75.995(2)	25.9198(8)	1.15703(4)	0.080524(3)
$\delta_{\mathrm{EW}}^{\mu^+\nu_\mu,\mathrm{var}}/\%$	-2.9	-5.0	-6.5	-8.0	-12.7	-16.8
$\delta_{\mathrm{EW}}^{\mathrm{rec},\mathrm{var}}/\%$	-1.9	-3.4	-4.9	-6.2	-10.1	-13.3
$\delta_{\mathrm{QCD}}^{\mu=M_{\mathrm{W}}}/\%$	33.8(1)	20.8(1)	12.5(1)	7.4(1)	$-4.7(1)$	$-13.2(1)$
$\delta_{\mathrm{QCD}}^{\mathrm{var}}/\%$	36.2(1)	24.5(1)	16.9(1)	12.4(1)	1.7(1)	$-5.9(1)$
$\delta_{\gamma,\mathrm{Born}}^{\mathrm{var}}/\%$	0.4	0.2	0.2	0.1	0.1	0.05
$\delta_{\gamma,\mathrm{NLO}}^{\mathrm{var}}/\%$	0.3	0.2	0.2	0.1	0.1	0.05
$\delta_{\mathrm{IF}}^{\mathrm{var}}/\%$	-0.1	-0.1	-0.1	-0.1	-0.1	-0.04

Table 5. Integrated cross sections for different cuts on the transverse mass of the W at the Tevatron.

3.4 Results on momentum and transverse-mass distributions

In figures 7–12 we show for various observables the LO distribution and the distribution including the full set of corrections, i.e. EW corrections δ_{EW}, the contribution of the photon-induced processes $\delta_{\gamma,\mathrm{NLO}}$, interference contribution δ_{IF}, and the QCD corrections. The various contributions to the corrections are also shown separately relative to the LO.

$p\bar{p} \to l^+\nu_l$ jet $+ X$ at $\sqrt{s} = 1.96\,\mathrm{TeV}$						
$p_{\mathrm{T,jet}}/\,\mathrm{GeV}$	$25 - \infty$	$50 - \infty$	$75 - \infty$	$100 - \infty$	$200 - \infty$	$300 - \infty$
$\sigma_{\mathrm{Born}}^{\mu = M_W}/\,\mathrm{fb}$	37341.5(7)	8848.7(2)	3115.31(6)	1231.80(2)	54.5590(8)	3.62805(6)
$\sigma_{\mathrm{Born}}^{\mathrm{var}}/\,\mathrm{fb}$	36056.0(7)	8094.1(2)	2686.10(5)	998.31(2)	34.9921(6)	1.89648(3)
$\delta_{\mathrm{EW}}^{\mu^+\nu_\mu,\mathrm{var}}/\%$	-2.8	-2.9	-3.2	-3.7	-6.5	-9.2
$\delta_{\mathrm{EW}}^{\mathrm{rec},\mathrm{var}}/\%$	-1.9	-2.2	-2.6	-3.2	-6.2	-9.0
$\delta_{\mathrm{QCD}}^{\mu = M_W}/\%$	33.5(1)	31.7(1)	25.1(1)	20.7(1)	6.2(1)	$-8.7(1)$
$\delta_{\mathrm{QCD}}^{\mathrm{var}}/\%$	36.3(1)	39.5(1)	39.5(1)	41.9(1)	56.6(1)	70.5(1)
$\delta_{\mathrm{QCD,veto}}^{\mu = M_W}/\%$	20.9(1)	7.4(1)	1.4(1)	$-3.7(1)$	$-24.0(1)$	$-43.8(1)$
$\delta_{\mathrm{QCD,veto}}^{\mathrm{var}}/\%$	24.0(1)	15.4(1)	15.2(1)	16.4(1)	19.7(1)	21.1(1)
$\delta_{\gamma,\mathrm{Born}}^{\mathrm{var}}/\%$	0.4	0.8	1.2	1.4	2.0	2.3
$\delta_{\gamma,\mathrm{NLO}}^{\mathrm{var}}/\%$	0.4	0.8	1.1	1.3	1.8	2.2
$\delta_{\gamma,\mathrm{NLO,veto}}^{\mathrm{var}}/\%$	0.4	0.7	1.0	1.3	1.8	2.1
$\delta_{\mathrm{IF}}^{\mathrm{var}}/\%$	-0.1	-0.4	-0.6	-0.8	-2.0	-3.5
$\delta_{\mathrm{IF,veto}}^{\mathrm{var}}/\%$	-0.04	-0.1	-0.3	-0.4	-0.7	-1.1

Table 6. Integrated cross sections for different cuts on the p_{T} of the leading jet at the Tevatron. Corrections with a second jet in real emission events are shown with and without a jet veto.

While the corrections to the integrated cross sections are quite similar for a given $p_{\mathrm{T},l}$ and an $M_{\mathrm{T},l\nu_l}$ cut of similar size, the differential distributions in figure 7 and figure 8 are significantly different. The EW corrections for the $M_{\mathrm{T},l\nu_l}$ distributions resemble the corrections for the inclusive W-boson sample for which no additional jet is required (see, e.g., figure 2 in ref. [14]). This result is expected since the definition (3.5) of the transverse mass is boost invariant to first order in the boost velocity and therefore insensitive to a boost of the intermediate W boson. The $p_{\mathrm{T},l}$ distribution, in contrast, is sensitive to these boosts, and neither the LO prediction nor the NLO EW corrections resemble the inclusive result (see, e.g., figure 1 in ref. [14]).

As expected, the corrections for bare muons are larger since photons, being radiated collinearly to the charged lepton, carry away transverse momentum. Hence, events that are enhanced by muon-mass logarithms are shifted to lower bins in the distributions and to some extent do not survive the basic cuts. As a result, the corrections are dominated by negative virtual corrections that are not compensated by positive bremsstrahlung contributions. This is particularly evident around the peak of the differential cross section with respect to the W-boson transverse mass in figure 8 and also for the peaks in the transverse-momentum distributions of the charged lepton near $(M_W \pm p_{\mathrm{T,jet}}^{\mathrm{cut}})/2$ in figure 7.

In figure 9 we show the differential cross sections with respect to $p_{\mathrm{T,jet}}$ and the corresponding corrections. As expected, the increasing size of the EW corrections with $p_{\mathrm{T,jet}}$ due
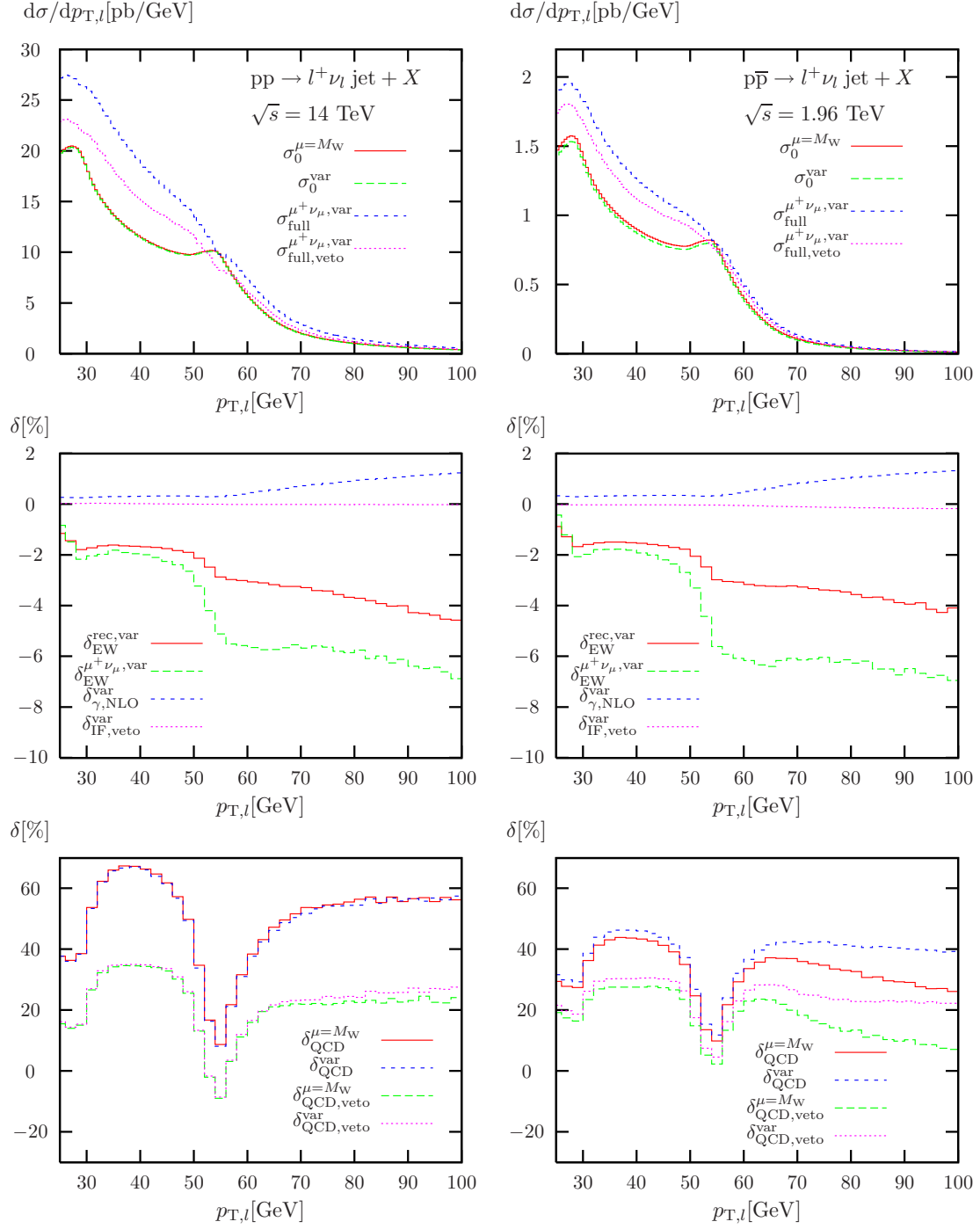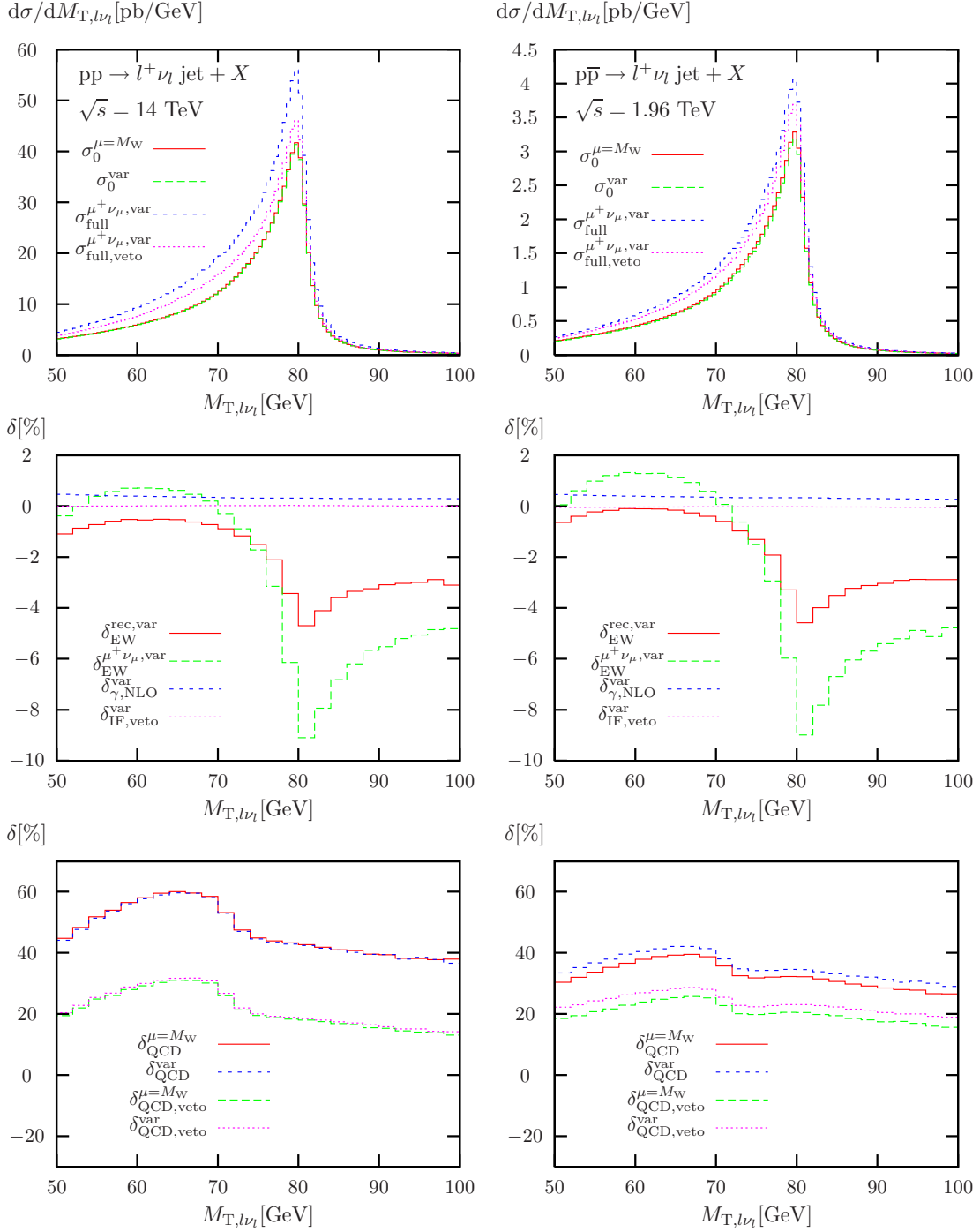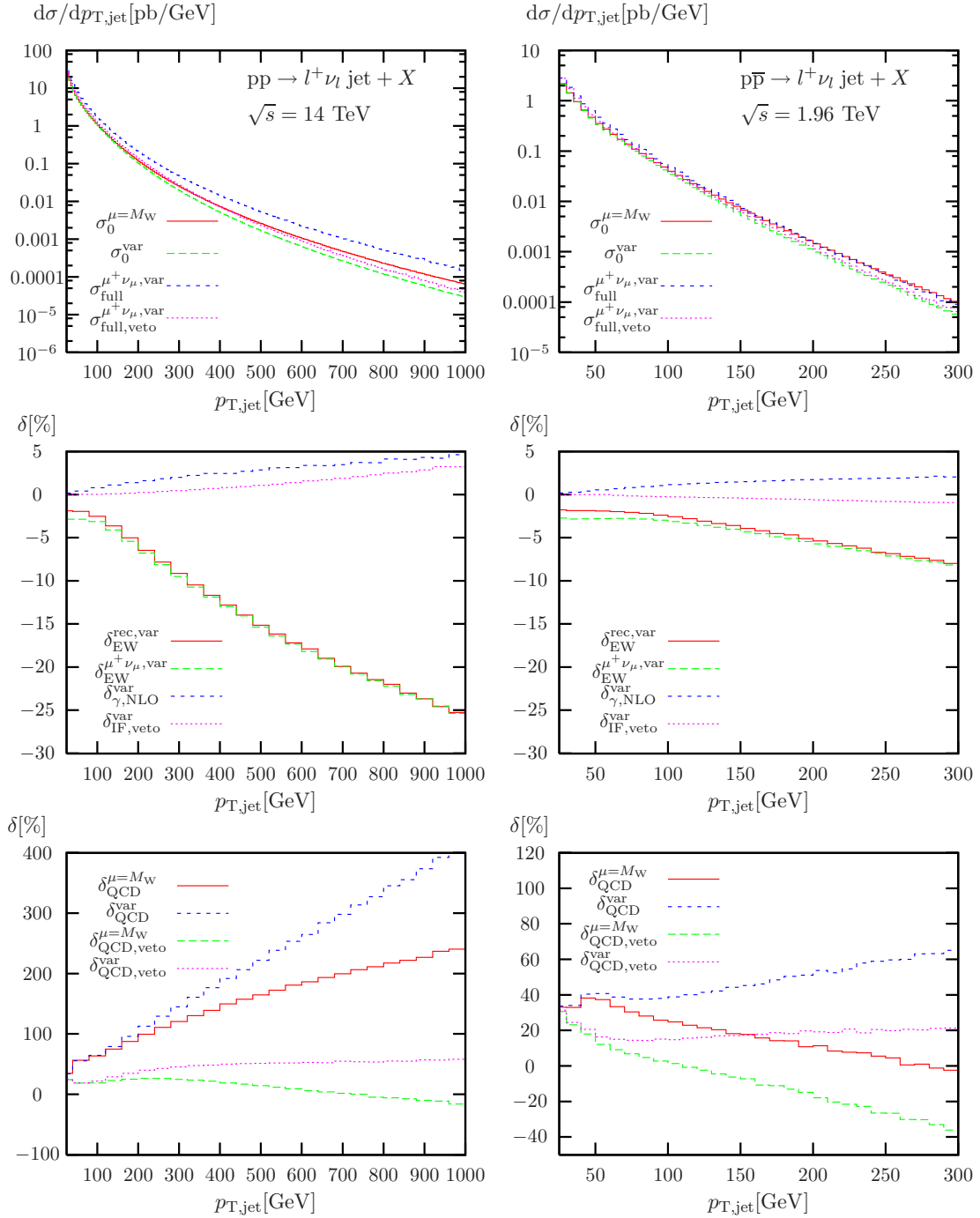
Figure 7. LO and fully corrected distribution (top), corresponding relative EW, photon-induced, and interference corrections (middle), and relative QCD corrections (bottom) for the transverse momentum of the charged lepton at the LHC (left) and the Tevatron (right).

to the EW Sudakov logarithms can be observed. This observable has also been accessible in calculations using the approximations of a stable, on-shell W boson. A comparison of our numerical results to former results for on-shell W + jet production [21–23] has to face the

Figure 8. LO and fully corrected distribution (top), corresponding relative EW, photon-induced, and interference corrections (middle), and relative QCD corrections (bottom) for the W transverse mass at the LHC (left) and the Tevatron (right).

problem that we apply various event-selection cuts to the leptonic final state, while in the previous papers the degrees of freedom related to the decaying W are implicitly integrated out. Nevertheless, the relative EW corrections at high momentum transfer are dominated

Figure 9. LO and fully corrected distribution (top), corresponding relative EW, photon-induced, and interference corrections (middle), and relative QCD corrections (bottom) for the the transverse momentum of the leading jet at the LHC (left) and the Tevatron (right).

by Sudakov logarithms of the form $\ln^2(\hat{s}/M_W^2)$ that, at least at the one-loop level, give rise to large process-independent contributions and therefore are expected to show a similar behaviour for both the on- and off-shell case. Comparing our results for the leading-jet

$p_{\mathrm{T,jet}}$ (figure 9) with figure 5 in ref. [22], we in fact find agreement within 2%. The results for the EW corrections to the integrated cross sections with different cuts on $p_{\mathrm{T,jet}}$ given in table 3 also agree within 1% with the results presented in figure 9(b) of ref. [23] for cut values larger than 200 GeV. This figure shows the relative corrections for the average of W$^+$- and W$^-$ production at the LHC, but the relative EW corrections to the on-shell W$^+$ and W$^-$ production rates turn out to be very similar, as can e.g. be seen in figure 10 of ref. [22]. Comparing the EW corrections at the Tevatron given in table 6 to the on-shell results of figure 9(a) in ref. [23], we observe slightly larger deviations, because the universal Sudakov-like contributions are not dominant at typical Tevatron energy scales.

Turning again to the NLO QCD results, the corrections to $p_{\mathrm{T},l}$ and $M_{\mathrm{T},l\nu_l}$ distributions, also displayed in figures 7 and 8, show quite different features. The corrections to the $M_{\mathrm{T},l\nu_l}$ distribution are flatter, reflecting the well-known fact that the transverse mass is less sensitive to additional QCD radiation. In contrast, the corrections δ_{QCD} for $p_{\mathrm{T},l}$ show pronounced dips where the LO cross section has peaks. The real corrections do not particularly populate the regions of the distributions that are enhanced due to the particular LO kinematics. The QCD corrections to the differential distribution for $p_{\mathrm{T,jet}}$ show exactly the same features which have already been discussed for the integrated cross sections (see table 3), as can be seen in figure 9.

At the Tevatron, the shapes of the EW and QCD corrections to distributions (see figures 7–9) are very similar to the respective results for the LHC. For the p_{T} distribution of the leading jet (see figure 9), the jet veto again stabilizes the perturbative result. However, using the variable scale choice, the increase in cross section without jet veto is not as pronounced as at the LHC. On the other hand, as expected, the fixed scale choice together with a jet veto leads to large negative corrections. A fixed scale choice without a jet veto accidentally leads to small corrections at the Tevatron.

3.5 Results on rapidity and angular distributions

In figure 10, we analyse the rapidity distribution for the charged lepton. While the EW corrections are flat, the NLO QCD corrections are larger at large rapidities and, hence, tend to populate the forward and backward regions with more events. Concerning the rapidity of the leading jet at the LHC, both EW and NLO QCD corrections do not disturb the LO shapes of the distribution, as can be seen in figure 11.

At the Tevatron, the rapidity distributions show the expected asymmetry between the forward and backward direction due to the antiproton in the initial state. This asymmetry is also reflected by asymmetric NLO QCD corrections for the rapidity of the leading jet.

Another interesting observable is the angle between the charged lepton and missing p_{T} in the transverse plane (figure 12). For W production without jet activity the two leptons are always back-to-back in the transverse plane. Here, with one jet at LO, the distribution is still peaked at large angles. However, back-to-back events are suppressed as shown in figure 12. While the EW corrections only slightly disturb the shape of the distribution, the NLO QCD corrections tend to distribute events more equally with respect to the investigated angle. However, the dip in the NLO distributions at the LO peak might indicate that higher orders are necessary for an accurate prediction of this observable. The shapes of the relative QCD corrections reflect the large impact of real corrections
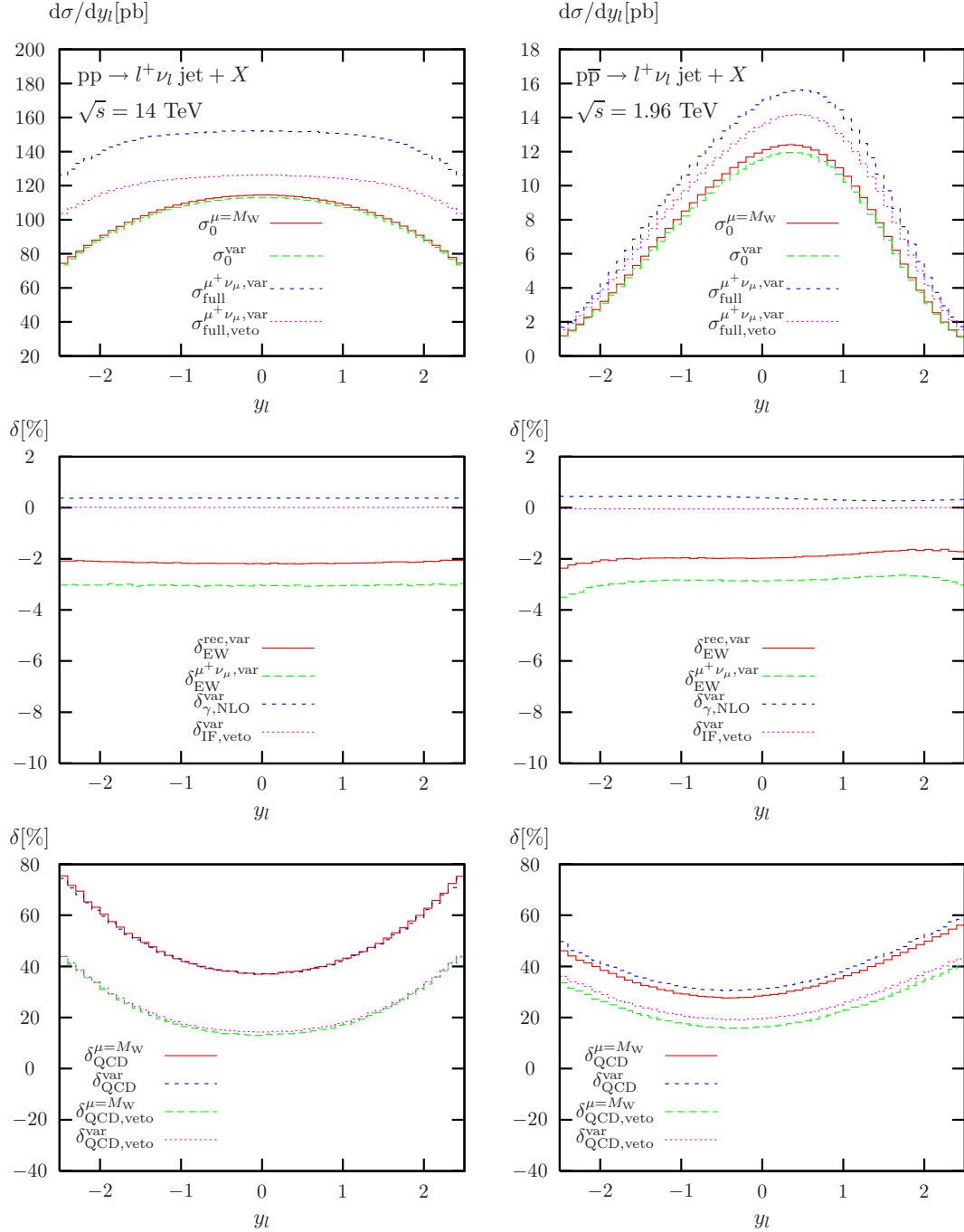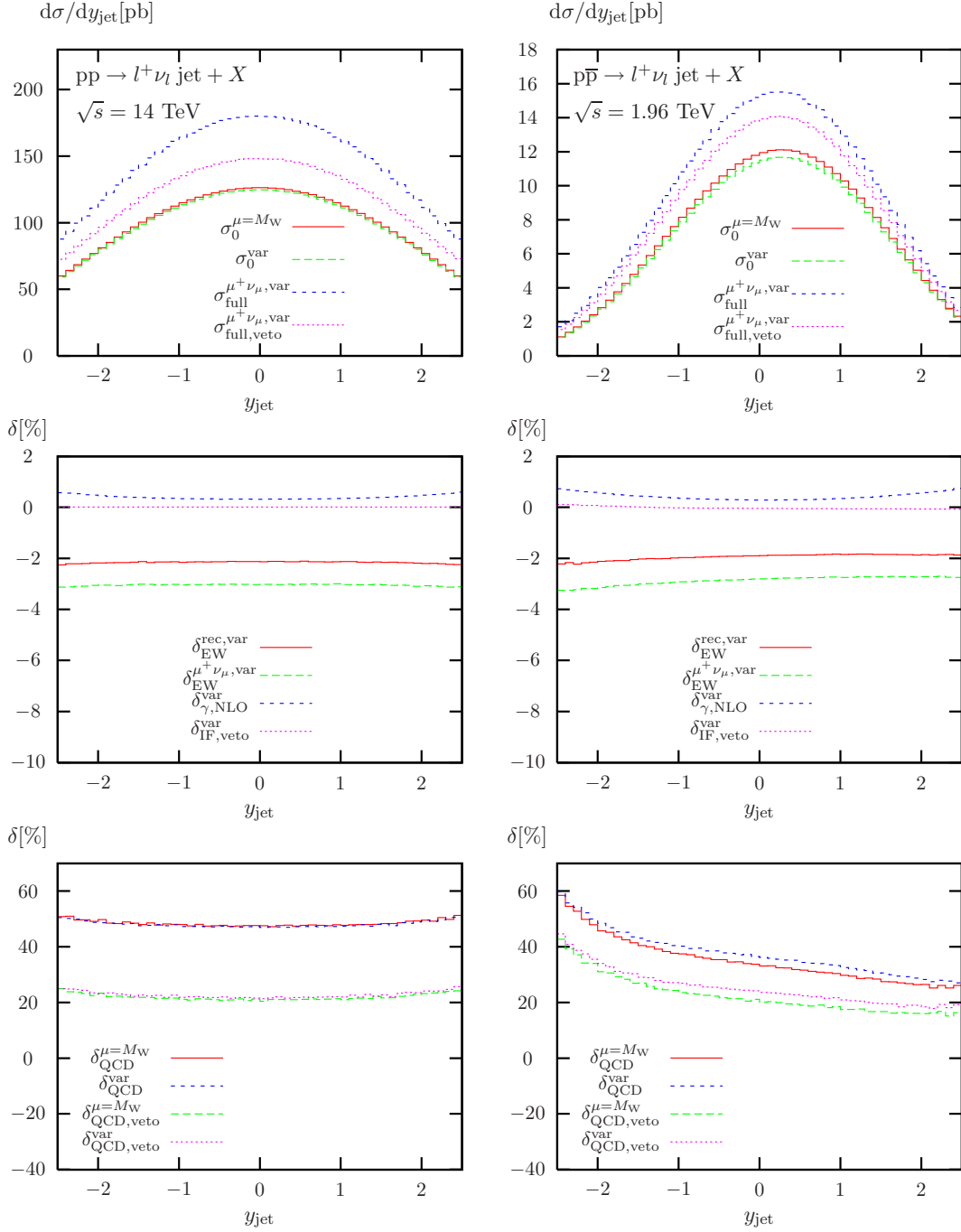
Figure 10. LO and fully corrected distribution (top), corresponding relative EW, photon-induced, and interference corrections (middle), and relative QCD corrections (bottom) for the rapidity of the charged lepton at the LHC (left) and the Tevatron (right).

induced by $W + 2$ jets configurations where two hard jets are nearly back-to-back while the W boson receives only a small transverse momentum. Such events cause the large positive corrections for $\phi_{l\nu_l} \rightarrow 180°$, which are sensitive to the application of the jet veto.

Figure 11. LO and fully corrected distribution (top), corresponding relative EW, photon-induced, and interference corrections (middle), and relative QCD corrections (bottom) for the rapidity of the leading jet at the LHC (left) and the Tevatron (right).

4 Conclusions

We have presented the first calculation of the full electroweak (EW) NLO corrections for W-boson hadroproduction in association with a hard jet where all off-shell effects are taken
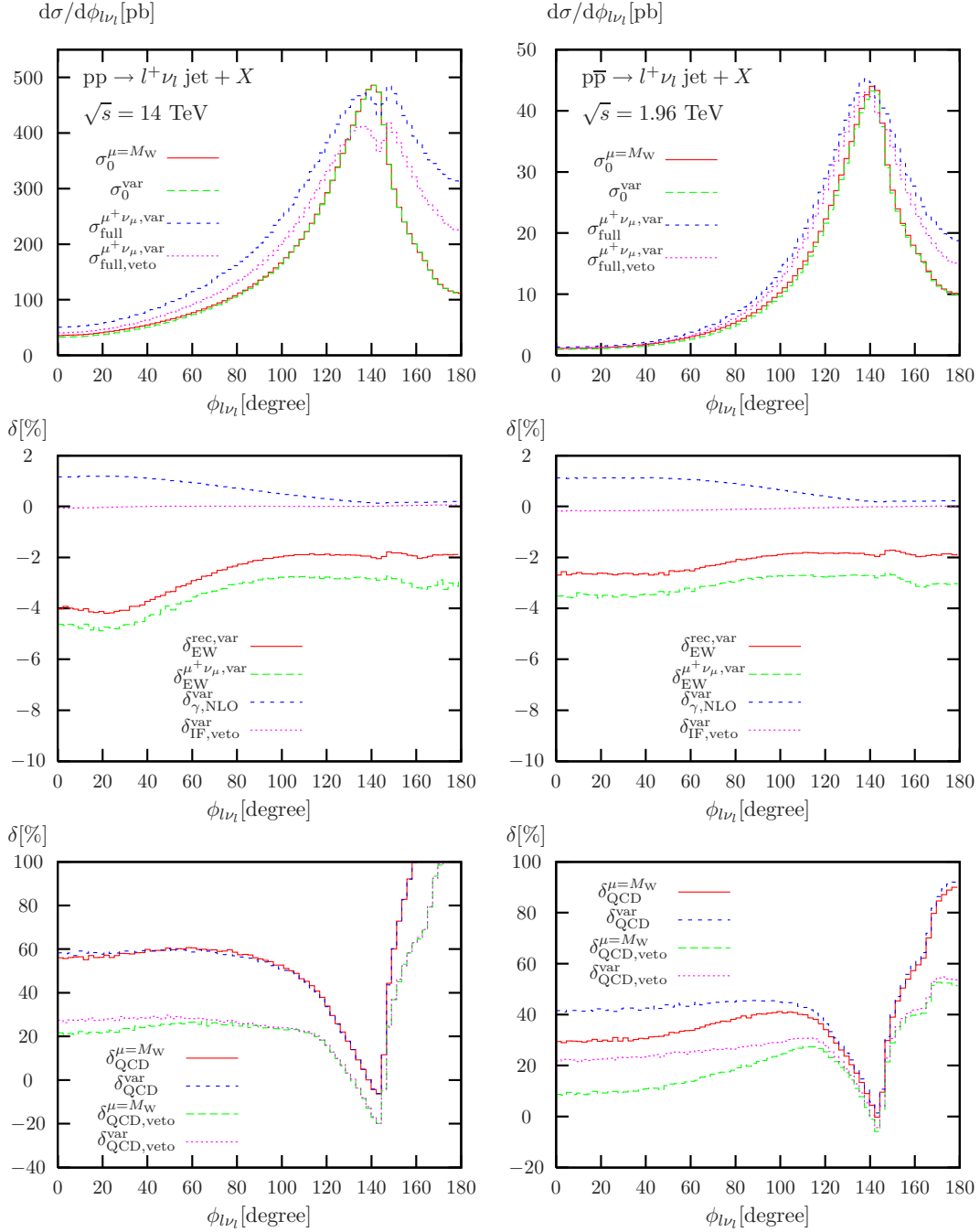
Figure 12. LO and fully corrected distribution (top), corresponding relative EW, photon-induced, and interference corrections (middle), and relative QCD corrections (bottom) for the azimuthal angle in the transverse plane between the charged lepton and the neutrino (missing p_T) at the LHC (left) and the Tevatron (right).

into account in the leptonic W-boson decay, i.e. we have studied final states with a jet, a charged lepton, and missing transverse momentum at NLO in the EW coupling constant within the SM.

We have implemented our results in a flexible Monte Carlo code which can model the experimental event definition at the NLO parton level. The distinction of W + jet and W + photon production is consistently implemented by making use of the measured quark-to-photon fragmentation function. We have also recalculated the NLO QCD corrections supporting a phase-space dependent scale choice. Interference contributions by EW and QCD diagrams as well as photon-induced processes, contributing at the same order, are included but phenomenologically unimportant.

The presented integrated cross sections and differential distributions demonstrate the applicability of our calculation. The EW corrections to the transverse mass of the W boson exhibit the same enhancement as for W bosons without jet activity, reaching -10% at the peak of the LO distribution which is dominated by resonant W bosons. For large transverse mass, i.e. in the off-shell tail of the distribution, we find large negative corrections, dominated by the well-known EW Sudakov logarithms. The EW corrections to the p_T distributions of the final-state particles are rather flat and at the percent level for small values of p_T and also become more and more negative owing to contributions from Sudakov logarithms in accordance with previous on-shell approximations. The QCD corrections have a typical size of 50%. However, they can become extremely large (hundreds of percent) at large jet p_T if one does not apply a sensible jet veto.

The precise prediction for W-boson production at the Tevatron and the LHC is an important task. Our results extend the theoretical effort to associated production with a hard jet. As part of a full NNLO prediction of the mixed EW and QCD corrections for inclusive W production our results can provide a handle for a better understanding of the interplay between EW and QCD corrections in the charged-current Drell-Yan process. Moreover, they establish a flexible precision calculation for one of the most important background processes for new-physics searches. In the range of intermediate and large transverse momenta of the additional hard jet our calculation delivers state-of-the-art predictions, for small transverse momenta the pure NLO calculation should of course be improved by dedicated QCD resummations, a task that goes beyond the scope of this paper.

Acknowledgments

References

[1] TeV4LHC-Top and Electroweak Working Group collaboration, C.E. Gerber et al., *Tevatron-for-LHC report: top and electroweak physics*, arXiv:0705.3251 [SPIRES].

[2] TeV4LHC Landscape Working Group collaboration, S. Abdullin et al., *Tevatron-for-LHC Report: preparations for discoveries*, hep-ph/0608322 [SPIRES].

[3] W.L. van Neerven and E.B. Zijlstra, *The $O(\alpha_s^2)$ corrected Drell-Yan K factor in the DIS and MS scheme*, *Nucl. Phys.* **B 382** (1992) 11 [*Erratum ibid.* **B 680** (2004) 513] [SPIRES];
R.V. Harlander and W.B. Kilgore, *Next-to-next-to-leading order Higgs production at hadron colliders*, *Phys. Rev. Lett.* **88** (2002) 201801 [hep-ph/0201206] [SPIRES];
C. Anastasiou, L.J. Dixon, K. Melnikov and F. Petriello, *Dilepton rapidity distribution in the Drell-Yan process at NNLO in QCD*, *Phys. Rev. Lett.* **91** (2003) 182002 [hep-ph/0306192] [SPIRES];
C. Anastasiou, L.J. Dixon, K. Melnikov and F. Petriello, *High precision QCD at hadron colliders: electroweak gauge boson rapidity distributions at NNLO*, *Phys. Rev.* **D 69** (2004) 094008 [hep-ph/0312266] [SPIRES];
S. Catani, L. Cieri, G. Ferrera, D. de Florian and M. Grazzini, *Vector boson production at hadron colliders: a fully exclusive QCD calculation at NNLO*, arXiv:0903.2120 [SPIRES].

[4] S. Moch and A. Vogt, *Higher-order soft corrections to lepton pair and Higgs boson production*, *Phys. Lett.* **B 631** (2005) 48 [hep-ph/0508265] [SPIRES];
E. Laenen and L. Magnea, *Threshold resummation for electroweak annihilation from DIS data*, *Phys. Lett.* **B 632** (2006) 270 [hep-ph/0508284] [SPIRES];
A. Idilbi, X. Ji, J.-P. Ma and F. Yuan, *Threshold resummation for Higgs production in effective field theory*, *Phys. Rev.* **D 73** (2006) 077501 [hep-ph/0509294] [SPIRES];
V. Ravindran and J. Smith, *Threshold corrections to rapidity distributions of Z and $W^{\pm}$ bosons beyond N^2LO at hadron colliders*, *Phys. Rev.* **D 76** (2007) 114004 [arXiv:0708.1689] [SPIRES].

[5] S. Frixione and B.R. Webber, *The MC@NLO 3.3 event generator*, hep-ph/0612272 [SPIRES];
S. Frixione, P. Nason and C. Oleari, *Matching NLO QCD computations with parton shower simulations: the POWHEG method*, *JHEP* **11** (2007) 070 [arXiv:0709.2092] [SPIRES];
S. Alioli, P. Nason, C. Oleari and E. Re, *NLO vector-boson production matched with shower in POWHEG*, *JHEP* **07** (2008) 060 [arXiv:0805.4802] [SPIRES].

[6] C. Balázs and C.P. Yuan, *Soft gluon effects on lepton pairs at hadron colliders*, *Phys. Rev.* **D 56** (1997) 5558 [hep-ph/9704258] [SPIRES];
R.K. Ellis and S. Veseli, *W and Z transverse momentum distributions: resummation in q_T space*, *Nucl. Phys.* **B 511** (1998) 649 [hep-ph/9706526] [SPIRES];
A. Kulesza and W.J. Stirling, *On the resummation of subleading logarithms in the transverse momentum distribution of vector bosons produced at hadron colliders*, *JHEP* **01** (2000) 016 [hep-ph/9909271] [SPIRES].

[7] S. Frixione and M.L. Mangano, *How accurately can we measure the W cross section?*, *JHEP* **05** (2004) 056 [hep-ph/0405130] [SPIRES].

[8] V.A. Zykunov, *Electroweak corrections to the observables of W-boson production at RHIC*, *Eur. Phys. J. direct* **C 3** (2001) 9 [hep-ph/0107059] [SPIRES].

[9] S. Dittmaier and M. Krämer, *Electroweak radiative corrections to W-boson production at hadron colliders*, *Phys. Rev.* **D 65** (2002) 073007 [hep-ph/0109062] [SPIRES].

[10] U. Baur and D. Wackeroth, *Electroweak radiative corrections to $p\bar{p} \to W^{\pm} \to \ell^{\pm}\nu$ beyond the pole approximation*, *Phys. Rev.* **D 70** (2004) 073015 [hep-ph/0405191] [SPIRES];
A. Arbuzov et al., *One-loop corrections to the Drell-Yan process in SANC. I: the charged current case*, *Eur. Phys. J.* **C 46** (2006) 407 [*Erratum ibid.* **C 50** (2007) 505] [hep-ph/0506110] [SPIRES].

[11] C.M. Carloni Calame, G. Montagna, O. Nicrosini and A. Vicini, *Precision electroweak calculation of the charged current Drell-Yan process*, *JHEP* **12** (2006) 016 [hep-ph/0609170] [SPIRES].

[12] C.M. Carloni Calame, G. Montagna, O. Nicrosini and M. Treccani, *Higher-order QED corrections to W-boson mass determination at hadron colliders*, *Phys. Rev.* **D 69** (2004) 037301 [hep-ph/0303102] [SPIRES].

[13] W. Placzek and S. Jadach, *Multiphoton radiation in leptonic W-boson decays*, *Eur. Phys. J.* **C 29** (2003) 325 [hep-ph/0302065] [SPIRES];
C.M. Carloni Calame, S. Jadach, G. Montagna, O. Nicrosini and W. Placzek, *Comparisons of the Monte Carlo programs HORACE and WINHAC for single W-boson production at hadron colliders*, *Acta Phys. Polon.* **B 35** (2004) 1643 [hep-ph/0402235] [SPIRES].

[14] S. Brensing, S. Dittmaier, M. Krämer and A. Mück, *Radiative corrections to W-boson hadroproduction: higher-order electroweak and supersymmetric effects*, *Phys. Rev.* **D 77** (2008) 073006 [arXiv:0710.3309] [SPIRES].

[15] S. Dittmaier and M. Krämer, DK results given in *Tuned comparison of electroweak corrections to DrellYan-like W- and Z-boson production – A status report*, in C. Buttar et al., *Les Houches physics at TeV colliders* 2005, *standard model and Higgs working group: summary report*, hep-ph/0604120 [SPIRES].

[16] A.B. Arbuzov and R.R. Sadykov, *Inverse bremsstrahlung contributions to Drell-Yan like processes*, *J. Exp. Theor. Phys.* **106** (2008) 488 [arXiv:0707.0423] [SPIRES].

[17] Q.-H. Cao and C.P. Yuan, *Combined effect of QCD resummation and QED radiative correction to W boson observables at the Tevatron*, *Phys. Rev. Lett.* **93** (2004) 042001 [hep-ph/0401026] [SPIRES];
B.F.L. Ward, C. Glosser, S. Jadach and S.A. Yost, *Threshold corrections in precision LHC physics: QED × QCD*, *Int. J. Mod. Phys.* **A 20** (2005) 3735 [hep-ph/0411047] [SPIRES];
B.F.L. Ward and S.A. Yost, *QED × QCD resummation and shower/ME matching for LHC physics*, *Acta Phys. Polon.* **B 38** (2007) 2395 [arXiv:0704.0294] [SPIRES];
A. Vicini et al., *Drell-Yan processes at the LHC*, PoS(RADCOR2007)013 [SPIRES];
G. Balossini et al., *Drell-Yan processes at hadron colliders*, *Nuovo Cim.* **123B** (2008) 741 [SPIRES].

[18] W.T. Giele, E.W.N. Glover and D.A. Kosower, *Higher order corrections to jet cross-sections in hadron colliders*, *Nucl. Phys.* **B 403** (1993) 633 [hep-ph/9302225] [SPIRES].

[19] J.M. Campbell and R.K. Ellis, *Next-to-leading order corrections to W+ 2 jet and Z+ 2 jet production at hadron colliders*, *Phys. Rev.* **D 65** (2002) 113007 [hep-ph/0202176] [SPIRES].

[20] R.K. Ellis, K. Melnikov and G. Zanderighi, *Generalized unitarity at work: first NLO QCD results for hadronic W+ 3 jet production*, *JHEP* **04** (2009) 077 [arXiv:0901.4101] [SPIRES];
C.F. Berger et al., *Precise predictions for W + 3 jet production at hadron colliders*, *Phys. Rev. Lett.* **102** (2009) 222001 [arXiv:0902.2760] [SPIRES].

[21] J.H. Kühn, A. Kulesza, S. Pozzorini and M. Schulze, *Electroweak corrections to large transverse momentum production of W bosons at the LHC*, *Phys. Lett.* **B 651** (2007) 160 [hep-ph/0703283] [SPIRES].

[22] J.H. Kühn, A. Kulesza, S. Pozzorini and M. Schulze, *Electroweak corrections to hadronic production of W bosons at large transverse momenta*, *Nucl. Phys.* **B 797** (2008) 27 [arXiv:0708.0476] [SPIRES].

[23] W. Hollik, T. Kasprzik and B.A. Kniehl, *Electroweak corrections to W-boson hadroproduction at finite transverse momentum*, *Nucl. Phys.* **B 790** (2008) 138 [`arXiv:0707.2553`] [SPIRES].

[24] G.J. Gounaris, J. Layssac and F.M. Renard, *Remarkable virtual SUSY effects in $W^{\pm}$ production at high energy hadron colliders*, *Phys. Rev.* **D 77** (2008) 013003 [`arXiv:0709.1789`] [SPIRES].

[25] P. Ciafaloni and D. Comelli, *Sudakov enhancement of electroweak corrections*, *Phys. Lett.* **B 446** (1999) 278 [`hep-ph/9809321`] [SPIRES];
V.S. Fadin, L.N. Lipatov, A.D. Martin and M. Melles, *Resummation of double logarithms in electroweak high energy processes*, *Phys. Rev.* **D 61** (2000) 094002 [`hep-ph/9910338`] [SPIRES];
A. Denner and S. Pozzorini, *One-loop leading logarithms in electroweak radiative corrections. I: results*, *Eur. Phys. J.* **C 18** (2001) 461 [`hep-ph/0010201`] [SPIRES];
W. Beenakker and A. Werthenbach, *Electroweak two-loop Sudakov logarithms for on-shell fermions and bosons*, *Nucl. Phys.* **B 630** (2002) 3 [`hep-ph/0112030`] [SPIRES];
A. Denner, M. Melles and S. Pozzorini, *Two-loop electroweak angular-dependent logarithms at high energies*, *Nucl. Phys.* **B 662** (2003) 299 [`hep-ph/0301241`] [SPIRES].

[26] A. Denner, S. Dittmaier, M. Roth and D. Wackeroth, *Predictions for all processes $e^+e^- \to 4$ fermions $+\gamma$*, *Nucl. Phys.* **B 560** (1999) 33 [`hep-ph/9904472`] [SPIRES].

[27] A. Denner, S. Dittmaier, M. Roth and L.H. Wieders, *Electroweak corrections to charged-current $e^+e^- \to 4$ fermion processes: technical details and further results*, *Nucl. Phys.* **B 724** (2005) 247 [`hep-ph/0505042`] [SPIRES].

[28] ALEPH collaboration, D. Buskulic et al., *First measurement of the quark to photon fragmentation function*, *Z. Phys.* **C 69** (1996) 365 [SPIRES].

[29] A.D. Martin, R.G. Roberts, W.J. Stirling and R.S. Thorne, *Parton distributions incorporating QED contributions*, *Eur. Phys. J.* **C 39** (2005) 155 [`hep-ph/0411040`] [SPIRES].

[30] J. Küblbeck, M. Böhm and A. Denner, *FeynArts: computer algebraic generation of Feynman graphs and amplitudes*, *Comput. Phys. Commun.* **60** (1990) 165 [SPIRES];
H. Eck and J. Küblbeck, *Guide to FeynArts* 1.0, University of Würzburg, Würzburg, Germany (1992).

[31] G.P. Lepage, *A new algorithm for adaptive multidimensional integration*, *J. Comput. Phys.* **27** (1978) 192 [SPIRES]; *Vegas: an adaptive multidimensional integration program*, CLNS-80/447 [SPIRES].

[32] T. Hahn, *Generating Feynman diagrams and amplitudes with FeynArts* 3, *Comput. Phys. Commun.* **140** (2001) 418 [`hep-ph/0012260`] [SPIRES];
T. Hahn and C. Schappacher, *The implementation of the minimal supersymmetric standard model in FeynArts and FormCalc*, *Comput. Phys. Commun.* **143** (2002) 54 [`hep-ph/0105349`] [SPIRES].

[33] T. Hahn and M. Pérez-Victoria, *Automatized one-loop calculations in four and D dimensions*, *Comput. Phys. Commun.* **118** (1999) 153 [`hep-ph/9807565`] [SPIRES].

[34] S. Dittmaier, *Weyl-van-der-Waerden formalism for helicity amplitudes of massive particles*, *Phys. Rev.* **D 59** (1999) 016007 [`hep-ph/9805445`] [SPIRES].

[35] E. Accomando, A. Denner and C. Meier, *Electroweak corrections to $W\gamma$ and $Z\gamma$ production at the LHC*, *Eur. Phys. J.* **C 47** (2006) 125 [`hep-ph/0509234`] [SPIRES].

[36] S. Dittmaier and M. Roth, *LUSIFER: a LUcid approach to SIx FERmion production*, *Nucl. Phys.* **B 642** (2002) 307 [hep-ph/0206070] [SPIRES].

[37] A. Denner and S. Dittmaier, *The complex-mass scheme for perturbative calculations with unstable particles*, *Nucl. Phys. Proc. Suppl.* **160** (2006) 22 [hep-ph/0605312] [SPIRES].

[38] A. Denner, S. Dittmaier, M. Roth and M.M. Weber, *Electroweak radiative corrections to $e^+e^- \to \nu\bar{\nu}H$*, *Nucl. Phys.* **B 660** (2003) 289 [hep-ph/0302198] [SPIRES].

[39] G. 't Hooft and M.J.G. Veltman, *Scalar one loop integrals*, *Nucl. Phys.* **B 153** (1979) 365 [SPIRES];
W. Beenakker and A. Denner, *Infrared divergent scalar box integrals with applications in the electroweak standard model*, *Nucl. Phys.* **B 338** (1990) 349 [SPIRES];
A. Denner, U. Nierste and R. Scharf, *A compact expression for the scalar one loop four point function*, *Nucl. Phys.* **B 367** (1991) 637 [SPIRES].

[40] S. Dittmaier, *Separation of soft and collinear singularities from one-loop N-point integrals*, *Nucl. Phys.* **B 675** (2003) 447 [hep-ph/0308246] [SPIRES].

[41] D.B. Melrose, *Reduction of Feynman diagrams*, *Nuovo Cim.* **40** (1965) 181 [SPIRES].

[42] A. Denner and S. Dittmaier, *Reduction of one-loop tensor 5-point integrals*, *Nucl. Phys.* **B 658** (2003) 175 [hep-ph/0212259] [SPIRES].

[43] A. Denner and S. Dittmaier, *Reduction schemes for one-loop tensor integrals*, *Nucl. Phys.* **B 734** (2006) 62 [hep-ph/0509141] [SPIRES].

[44] G. Passarino and M. Veltman, *One loop corrections for e^+e^- annihilation into $\mu^+\mu^-$ in the Weinberg model*, *Nucl. Phys.* **B 160** (1979) 151 [SPIRES].

[45] A. Bredenstein, A. Denner, S. Dittmaier and S. Pozzorini, *NLO QCD corrections to top anti-top bottom anti-bottom production at the LHC: 1. quark-antiquark annihilation*, *JHEP* **08** (2008) 108 [arXiv:0807.1248] [SPIRES].

[46] S. Dittmaier, *A general approach to photon radiation off fermions*, *Nucl. Phys.* **B 565** (2000) 69 [hep-ph/9904440] [SPIRES].

[47] S. Dittmaier, A. Kabelschacht and T. Kasprzik, *Polarized QED splittings of massive fermions and dipole subtraction for non-collinear-safe observables*, *Nucl. Phys.* **B 800** (2008) 146 [arXiv:0802.1405] [SPIRES].

[48] K.P.O. Diener, S. Dittmaier and W. Hollik, *Electroweak higher-order effects and theoretical uncertainties in deep-inelastic neutrino scattering*, *Phys. Rev.* **D 72** (2005) 093002 [hep-ph/0509084] [SPIRES].

[49] T. Kinoshita, *Mass singularities of Feynman amplitudes*, *J. Math. Phys.* **3** (1962) 650 [SPIRES];
T.D. Lee and M. Nauenberg, *Degenerate systems and mass singularities*, *Phys. Rev.* **133** (1964) B1549 [SPIRES].

[50] E.A. Kuraev and V.S. Fadin, *On radiative corrections to e^+e^- single photon annihilation at high-energy*, *Sov. J. Nucl. Phys.* **41** (1985) 466 [*Yad. Fiz.* **41** (1985) 733] [SPIRES];
G. Altarelli and G. Martinelli, *Radiative corrections to the Z^0 line shape at LEP*, in *Physics at LEP*, volume 1, J. Ellis and R.D. Peccei eds., (1986) pag. 47 [SPIRES];
O. Nicrosini and L. Trentadue, *Soft photons and second order radiative corrections to $e^+e^- \to Z^0$*, *Phys. Lett.* **B 196** (1987) 551 [SPIRES]; *Second order electromagnetic radiative corrections to $e^+e^- \to \gamma^*, Z^0 \to \mu^+\mu^-$*, *Z. Phys.* **C 39** (1988) 479 [SPIRES];

F.A. Berends, W.L. van Neerven and G.J.H. Burgers, *Higher order radiative corrections at LEP energies*, *Nucl. Phys.* **B 297** (1988) 429 [*Erratum ibid.* **B 304** (1988) 921] [SPIRES];
A.B. Arbuzov, *Non-singlet splitting functions in QED*, *Phys. Lett.* **B 470** (1999) 252 [hep-ph/9908361] [SPIRES].

[51] E.W.N. Glover and A.G. Morgan, *Measuring the photon fragmentation function at LEP*, *Z. Phys.* **C 62** (1994) 311 [SPIRES].

[52] S. Catani and M.H. Seymour, *A general algorithm for calculating jet cross sections in NLO QCD*, *Nucl. Phys.* **B 485** (1997) 291 [*Erratum ibid.* **B 510** (1998) 503] [hep-ph/9605323] [SPIRES].

[53] PARTICLE DATA GROUP collaboration, C. Amsler et al., *Review of particle physics*, *Phys. Lett.* **B 667** (2008) 1 [SPIRES].

[54] D.Y. Bardin, A. Leike, T. Riemann and M. Sachwitz, *Energy dependent width effects in e^+e^- annihilation near the Z pole*, *Phys. Lett.* **B 206** (1988) 539 [SPIRES].

[55] C.W. Bauer and B.O. Lange, *Scale setting and resummation of logarithms in $pp \to V + jets$*, arXiv:0905.4739 [SPIRES].

[56] G.C. Blazey et al., *Run II jet physics*, hep-ex/0005012 [SPIRES].